

Effects of electron-electron interaction and spin-orbit coupling on Andreev pair qubits in quantum dot Josephson junctions

Teodor Iličin^{1,2,*}, Rok Žitko^{1,†}

¹ Jožef Stefan Institute, Jamova 39, SI-1000 Ljubljana, Slovenia

² Faculty of mathematics and physics, University of Ljubljana, Jadranska 19, SI-1000 Ljubljana, Slovenia

* teodor.ilicin@ijs.si † rok.zitko@ijs.si

Abstract

We investigate the superconducting Anderson impurity model for interacting quantum dot Josephson junctions with spin-orbit coupling and a term accounting for tunnelling through higher-energy orbitals. These elements establish the conditions required for spin polarization in the absence of external magnetic field at finite superconducting phase bias. This Hamiltonian has been previously used to model the Andreev spin qubit, where quantum information is encoded in spinful odd-parity subgap states. Here we instead analyse the even-parity sector, i.e., the Andreev pair qubit based on Andreev bound states (ABS). The model is solved using the zero-bandwidth approximation and the numerical renormalization group, with further insight from variational calculations. Electron-electron interaction admixes single-occupancy Yu-Shiba-Rusinov (YSR) components into the ABS states, thereby strongly enhancing spin transitions in the presence of spin-orbit coupling. The ABS states can thus become sensitive to local magnetic field fluctuations, which has implications for decoherence in Andreev pair qubits. For strong interaction U , especially in the cross-over region between the ABS and YSR regimes for $U \sim 2\Delta$, charge, spin, and inductive transitions can all become strong, offering avenues for spin control and quantum transduction.

Copyright attribution to authors.

This work is a submission to SciPost Physics.

License information to appear upon publication.

Publication information to appear upon publication.

Received Date

Accepted Date

Published Date

Contents

1	Introduction	2
2	Model	3
2.1	Parameter values	5
3	Methods	5
3.1	Zero-bandwidth approximation	5
3.2	Numerical renormalization group	5
3.3	Variational method	6
4	General considerations	7
4.1	Symmetry properties	7

4.2	Transition range between the ABS and YSR regimes	8
4.3	Emergence of local spin polarization	9
5	Results	9
5.1	Local-moment fraction	9
5.2	Magnetic response	11
5.3	Pairing properties	12
5.4	Energy separation	15
5.5	Transition matrix elements	17
5.6	NRG validation	17
6	Discussion: design implications	22
7	Conclusion	22
A	Variational approach	22
A.1	Variational equations	22
A.2	Wave-function properties and crossover between regimes	25
A.3	Away from half filling	26
A.4	Background tunneling processes	27
A.5	Spin-orbit coupling	28
	References	29

1 Introduction

Andreev level qubits store quantum information in the discrete subgap states localized at Josephson junctions between superconducting leads. The information can be encoded in different ways, either in the odd-occupancy subspace (Andreev spin qubits) [1–7] or in the even-occupancy subspace (Andreev pair qubits) [8–16]. In the case of Andreev pair qubits based on the Andreev bound states (ABS), the two basis states are distinguished by the relative phase of the empty-orbital and two-electron parts of the local wavefunction, $(|0\rangle \pm |2\rangle)/\sqrt{2}$, or equivalently, in the basis of Bogoliubov excitations, by the absence or presence of two trapped quasiparticles (QPs), see Fig. 1. One possible implementation of Andreev level qubits uses hybrid semiconductor-superconductor structures to build quantum-dot (QD) Josephson junctions that can trap QPs, for instance using InAs nanowires or Ge quantum wells [16–22]. Such structures can be modelled using the superconducting Anderson impurity model [23, 24]. Electrons confined in the QD experience Coulomb interaction, the strength of which, U , depends strongly on the material properties, the device geometry, and the tuning of gate voltages. It can range from very small values, in which case the interaction effects require some effort to be detected, to values where the nature of the subgap states changes completely and the QD behaves as a local magnetic moment; this is the regime of Yu-Shiba-Rusinov (YSR) states [22, 25–27]. The change occurs for values $U \approx 2\Delta$, where Δ is the superconducting gap [27]. In the limit of small hybridization strength Γ , the transition between the two limits is sharp; however, for experimentally relevant couplings it becomes continuous, accompanied by a strong mixing between the ABS and YSR components of the wavefunction [27], as schematically represented in Fig. 1. As a result, in presence of electron-electron (e-e) interaction the ABS states gen-

erally acquire some local-moment character and are therefore sensitive to magnetic fields. The implications of this mixed ABS/YSR character in realistic devices remain little explored, although the e-e interaction clearly affects the device response [4, 5, 20, 28–34]. In particular, the magnetic-field dependence of the ABS energy can induce unexpectedly large dephasing through local magnetic field fluctuations. Conversely, the coupling of even-parity subgap states to the magnetic field may prove advantageous, enabling magnetic state manipulation—akin to that in Andreev spin qubits—or supporting sensing and quantum transduction applications.

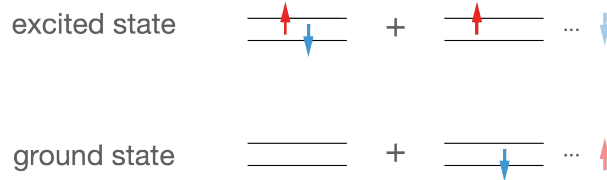


Figure 1: Schematic representation of the sub-gap states in the even-parity subsector. The lines represent the QD levels, the arrows represent Bogoliubov quasiparticles located either inside the junction (dark) or in the bath (light). The ABS components (left) differ in the number (zero or two) of trapped quasiparticles, the YSR components (right) differ in the wavefunction of the quasiparticle in the bath.

In this work we investigate the properties of superconducting Anderson impurity model that is extended in a minimal way to obtain chiral Andreev states [35, 36], as required to account for the spin-splitting of Andreev levels in the absence of the magnetic field. The extension is based on the idea of integrating out all other higher-energy levels in the QD beyond the partly occupied ("active") level closest to the Fermi level [5]. This leads to what may be denoted as "background tunnelling", which takes place alongside the main transport channel through the active level. These effects are captured in the effective Hamiltonian by a direct tunnelling term between the superconductors, which results from integrating out additional QD degrees of freedom [5]. Furthermore, the model includes spin-orbit coupling (SOC) [13, 37–41] and e-e interactions [42, 43], both of which are key for understanding Andreev spectra in real hybrid Josephson junctions [33]. This model has been previously applied to investigate the Andreev spin qubits [5]. In this work, we explore state composition, magnetic response, pairing properties, and energy separation of the even-parity subgap states. To evaluate the practical impact of interaction-induced local-moment components admixed into the ABS wavefunctions, we also compute the matrix elements of on-site spin operators and compare them with the corresponding matrix elements for charge and inductive transitions.

As key results, we will demonstrate that 1) because ABS acquire YSR admixture due to interaction, even-parity Andreev pair qubits are not purely charge qubits, but carry some local-moment character, 2) spin-orbit coupling in combination with chirality generates spin polarization and strong spin transition without external magnetic field, and 3) in the cross-over regime around $U \approx 2\Delta$, charge, spin, and inductive transition matrix elements can be large and tunable.

2 Model

We consider the situation where a single localized level in the QD embedded in the Josephson junction (JJ) dominates the low-energy physics. The Hamiltonian is then

$$\begin{aligned}
H = & \frac{U}{2}(\hat{n} - \nu)^2 + \sum_{lk\sigma} \epsilon_k c_{lk\sigma}^\dagger c_{lk\sigma} + \sum_{lk} \left(\Delta e^{i\phi_l} c_{lk\uparrow}^\dagger c_{lk\downarrow}^\dagger + \text{H.c.} \right) \\
& + \sum_{lk\sigma} \left(\frac{V_l^{(N)}}{\sqrt{N}} c_{lk\sigma}^\dagger d_\sigma + \text{H.c.} \right) + \sum_{lk\sigma} \left(\frac{V_l^{(\text{SF})}}{\sqrt{N}} c_{lk\sigma}^\dagger d_{\bar{\sigma}} + \text{H.c.} \right) + \sum_{kq\sigma} \left(\frac{V^{(D)}}{N} c_{Lk\sigma}^\dagger c_{Rq\sigma} + \text{H.c.} \right) \quad (1) \\
& + g_{\text{eff}} \mu_B (B_x S_x + B_y S_y + B_z S_z).
\end{aligned}$$

Here U is the electron–electron (e-e) repulsion, $\hat{n} = \sum_\sigma d_\sigma^\dagger d_\sigma$ is the QD occupancy operator for the orbital d (the partially occupied active level), ν is the gate voltage expressed in electron units (with $\nu = 1$ corresponding to nominal half filling of the QD). $l = L, R$ indexes the two superconducting leads, assumed to have equal dispersion ϵ_k , equal superconducting gap amplitude Δ , but different phases ϕ_l . We define $\phi = \phi_R - \phi_L$. The remaining terms describe electron transfer processes: $V^{(N)}$ and $V^{(\text{SF})}$ are the spin-conserving and spin-flipping tunneling amplitudes (the notation $\bar{\sigma}$ stands for spin inversion), while the $V^{(D)}$ term encodes all background tunnelling processes through the "inactive" orbitals away from the Fermi level (those that are nearly fully occupied or nearly empty). These orbitals are assumed to be integrated out, so that the only remaining contribution is this direct inter-lead hopping. This contribution to the Hamiltonian is important as a means to include the hybridisation chirality, which is a prerequisite for "spontaneous" spin polarization in the absence of external magnetic field [35–37]. Note that in most circumstances a nanowire Josephson junction will have a significant number of "inactive" orbitals, hence the $V^{(D)}$ term is generically expected to be present and need not be small, as evidenced by the properties of experimental devices that show large mesoscopic variability with many tuning points exhibiting very large spin splitting [5]. $V^{(D)}$ processes are assumed to be spin-conserving (without loss of generality). We will assume that the g -factor at the QD is significantly larger than that in the SC, thus the Zeeman term is included only at the QD orbital; g_{eff} is then the effective g -factor (essentially the difference of QD and SC g -factors). μ_B is the Bohr magneton.

We assume $V_l^{(N)}$ to be real and to have equal value for both leads. $V_l^{(\text{SF})}$ is assumed purely imaginary and of opposite signs, $V_L^{(\text{SF})} = -V_R^{(\text{SF})}$; the sign choice is important because spin-flip tunnelling terms are "directional". This choice maximizes the hybridization chirality. In matrix notation, the tunnelling terms can be expressed in the form

$$H' = \left(c_{lk\uparrow}^\dagger, c_{lk\downarrow}^\dagger \right) \left(V^{(N)} + \sigma_x V^{(\text{SF})} \right) \left(d_\uparrow, d_\downarrow \right)^T + \text{H.c.}, \quad (2)$$

where σ_x is the Pauli X matrix; the effective SOC field thus points along the x -axis. This specific choice of the SOC matrix has been made for notational and computational convenience and does not restrict generality; for a different orientation of the SOC field, one can choose the spin quantization axis so as to obtain this form.

To facilitate the discussion, we introduce the relative strength of the spin-flip terms (and thus the amplitude of the SOC effects) through a dimensionless ratio λ , so that

$$V_L^{(N)} = V_R^{(N)} = V(1 - \lambda), \quad V_L^{(\text{SF})} = -V_R^{(\text{SF})} = iV\lambda. \quad (3)$$

The parameter V encodes the overall hybridisation strength. The background tunnelling will be parametrized as

$$V^{(D)} = \tau V, \quad (4)$$

where τ quantifies the relative importance of tunnelling through higher-energy QD levels [5].

In many experimental devices multiple subgap modes are observed. In this work we focus on the minimal situation where a single localized level dominates the low-energy physics; multi-orbital effects are neglected and could modify quantitative details.

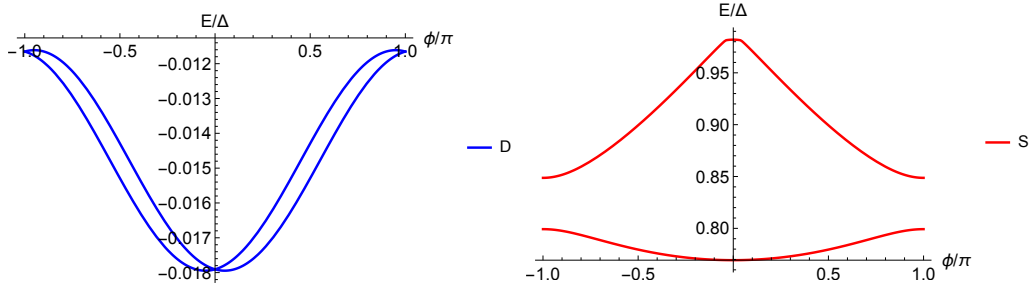


Figure 2: Energy-phase relationships (dispersion curves) of the "doublet" (odd parity, the states relevant in the Andreev spin qubit) and "singlet" (even parity, the states relevant in the Andreev pair qubit) subgap states for the reference set of parameters. (ZBW results)

2.1 Parameter values

In a realistic hybrid nanowire JJ device operated at a generic tuning point, no parameter is particularly small and all terms in the Hamiltonian are relevant. This is especially important for the formation of local moments and spin polarization in the ABS states. Experiments (Refs. [4, 5]) show a large mesoscopic variability of parameters, including the ratio of spin-preserving and spin-flip tunneling, implying that λ can take essentially arbitrary value. Unless stated otherwise, we will use the following parameters (referred to as "reference values"): interaction strength $U = 2\Delta$, overall hybridisation $V = 0.2\Delta$, nominal filling $\nu = 1$, dimensionless spin-orbit coupling $\lambda = 0.3$, ratio of background tunnelling $\tau = 0.4$, and phase bias $\phi = 0.75\pi$. The corresponding energy-phase relationships are shown in Fig. 2; in particular, the odd-parity states display the expected spin-splitting. Compared to experiments, this represents a modest splitting, thus the parameter set (including V and τ) is realistic and does not correspond to some extreme situation.

3 Methods

3.1 Zero-bandwidth approximation

We introduce the orbitals $f_{L\sigma} = \frac{1}{\sqrt{N}} \sum_k c_{Lk\sigma}$, $f_{R\sigma} = \frac{1}{\sqrt{N}} \sum_k c_{Rk\sigma}$, N being the number of orbitals in each superconducting band. By rewriting the tunnelling part of the Hamiltonian in terms of these operators and dropping from consideration all other orbitals in the superconductors, we obtain the zero-bandwidth (ZBW) Hamiltonian [44]. This approximation captures the essence of the problem and provides a convenient starting point for more controlled approaches [45]. For the present problem, comparison with NRG (next subsection) for representative parameter sets shows that the ZBW method captures all qualitative features of interest and can therefore be used reliably for mapping out trends. The ZBW calculations reduce to diagonalisation of small matrices.

3.2 Numerical renormalization group

For a fully quantitative description, especially of phenomena near $U \approx 2\Delta$ where discrete states interact with the continuum (which is beyond the ZBW approximation), we employ the numerical renormalization group (NRG) [46, 47]. NRG relies on logarithmic discretization of the leads, mapping to a Wilson chain, and iterative diagonalization. In the present case, the

method is particularly demanding due to the absence of symmetries beyond fermionic parity¹, which can be mitigated by using a coarser discretization parameter at the cost of somewhat larger systematic errors. Specifically, we use $\Lambda = 8$ and we keep up to 3000 states per iteration. Past experience shows that using large values of Λ does not lead to significant errors (in particular not to qualitative errors) [48, 49]. Even with such large Λ memory requirements are significant, on the order of 20 to 30GB. The calculation takes on the order of 3 to 4 hours for each parameter set when running on 8 cores of a modern CPU.

3.3 Variational method

In Ref. [27] we have recently proposed a variational Ansatz for solving the single-channel SC AIM for any value of U , from the ABS to the YSR limit. In this work, we generalize this approach to the two-channel case as appropriate for a Josephson junction. The Ansatz becomes $|\Psi\rangle = \sum_s |\varphi^s\rangle + \sum_l |\psi_l\rangle + \sum_{s,l,l'} |\chi_{l,l'}^s\rangle$, that contains wavefunctions with up to two QPs in the leads:

$$\begin{aligned}
|\varphi^+\rangle &= \frac{a^+}{\sqrt{2}} (1 + d_\uparrow^\dagger d_\downarrow^\dagger) |\Phi_0\rangle, \\
|\varphi^-\rangle &= \frac{a^-}{\sqrt{2}} (1 - d_\uparrow^\dagger d_\downarrow^\dagger) |\Phi_0\rangle, \\
|\psi_L\rangle &= \sum_k \frac{\alpha_{Lk}}{\sqrt{2}} (d_\uparrow^\dagger \gamma_{Lk\downarrow}^\dagger - d_\downarrow^\dagger \gamma_{Lk\uparrow}^\dagger) |\Phi_0\rangle, \\
|\psi_R\rangle &= \sum_k \frac{\alpha_{Rk}}{\sqrt{2}} (d_\uparrow^\dagger \gamma_{Rk\downarrow}^\dagger - d_\downarrow^\dagger \gamma_{Rk\uparrow}^\dagger) |\Phi_0\rangle, \\
|\chi_{LL}^\pm\rangle &= \sum_{k,q} \frac{\beta_{LLkq}^\pm}{2\sqrt{2}} (1 \pm d_\uparrow^\dagger d_\downarrow^\dagger) (\gamma_{Lk\uparrow}^\dagger \gamma_{Lq\downarrow}^\dagger - \gamma_{Lk\downarrow}^\dagger \gamma_{Lq\uparrow}^\dagger) |\Phi_0\rangle, \\
|\chi_{RR}^\pm\rangle &= \sum_{k,q} \frac{\beta_{RRkq}^\pm}{2\sqrt{2}} (1 \pm d_\uparrow^\dagger d_\downarrow^\dagger) (\gamma_{Rk\uparrow}^\dagger \gamma_{Rq\downarrow}^\dagger - \gamma_{Rk\downarrow}^\dagger \gamma_{Rq\uparrow}^\dagger) |\Phi_0\rangle, \\
|\chi_{LR}^\pm\rangle &= \sum_{k,q} \frac{\beta_{LRkq}^\pm}{2} (1 \pm d_\uparrow^\dagger d_\downarrow^\dagger) (\gamma_{Lk\uparrow}^\dagger \gamma_{Rq\downarrow}^\dagger - \gamma_{Lk\downarrow}^\dagger \gamma_{Rq\uparrow}^\dagger) |\Phi_0\rangle.
\end{aligned} \tag{5}$$

Here $\gamma_{lk\sigma}$ is the annihilation operator for a Bogoliubov QP in lead $l \in \{L, R\}$ with momentum k and spin σ , defined in Appendix A. Note that there are six independent two-QP states, corresponding to $(l, l') = (L, L), (R, R), (L, R)$, each combination occurring with a +1 and -1 relative sign in the ABS part of the wavefunction. The numerical prefactors in the Ansatz have been chosen such that the wavefunction is normalized as

$$|a^+|^2 + |a^-|^2 + \sum_{lk} (|\alpha_{lk}^+|^2 + |\alpha_{lk}^-|^2) + \sum_{(l'l')kk'} (|\beta_{l'l'kk'}^+|^2 + |\beta_{l'l'kk'}^-|^2) = 1, \tag{6}$$

where $(l'l')$ corresponds to enumeration over the three combinations of lead indexes. The indexes β_{ll} are symmetric in momentum indexes: $\beta_{llkq} = \beta_{llqk}$. In the presence of spin-orbit coupling, the Ansatz needs to be extended with spin-triplet counterparts to $|\psi_L\rangle, |\psi_R\rangle, |\chi_{l'l'}^\pm\rangle$. For the particular choice of spin-flip tunneling terms with SOC effective field direction along the x -axis, it is convenient to work with the eigenstates of the x -component of the total spin

¹For zero magnetic field, one could make use of the conserved x -component of total spin. However, magnetic field along the z -axis is required to extract the strength of the SOC effective field.

operator S_x . With our choice of the hopping terms, only the $S_x = 0$ terms are required:

$$\begin{aligned}
|\psi_L^T\rangle &= \sum_k \frac{\alpha_{Lk}^T}{\sqrt{2}} (d_{\uparrow}^{\dagger} \gamma_{Lk\uparrow}^{\dagger} - d_{\downarrow}^{\dagger} \gamma_{Lk\downarrow}^{\dagger}) |\Phi_0\rangle, \\
|\psi_R^T\rangle &= \sum_k \frac{\alpha_{Rk}^T}{\sqrt{2}} (d_{\uparrow}^{\dagger} \gamma_{Rk\uparrow}^{\dagger} - d_{\downarrow}^{\dagger} \gamma_{Rk\downarrow}^{\dagger}) |\Phi_0\rangle, \\
|\chi_{ll}^{\pm, T}\rangle &= \sum_{k,q} \frac{\xi_{llkq}^{\pm}}{2} (1 \pm d_{\uparrow}^{\dagger} d_{\downarrow}^{\dagger}) (\gamma_{lk\uparrow}^{\dagger} \gamma_{lq\uparrow}^{\dagger} - \gamma_{lk\downarrow}^{\dagger} \gamma_{lq\downarrow}^{\dagger}) |\Phi_0\rangle, \\
|\chi_{LR}^{\pm, T}\rangle &= \sum_{k,q} \frac{\xi_{LRkq}^{\pm}}{\sqrt{2}} (1 \pm d_{\uparrow}^{\dagger} d_{\downarrow}^{\dagger}) (\gamma_{Lk\uparrow}^{\dagger} \gamma_{Rq\uparrow}^{\dagger} - \gamma_{Lk\downarrow}^{\dagger} \gamma_{Rq\downarrow}^{\dagger}) |\Phi_0\rangle,
\end{aligned} \tag{7}$$

Further details about the method are provided in Appendix A. We will mostly use the variational method for qualitative guidance: the results presented in the figures in the main text are obtained using the ZBW and NRG. In particular limits, the variational solution becomes simple, allowing us to transparently write the quantitatively correct wave-functions. These results are then used to provide further clarification of the qualitative behaviour observed in the numerical (ZBW and NRG) results.

4 General considerations

4.1 Symmetry properties

For general parameters, the Hamiltonian has very little symmetry: only the x component of the total spin is conserved (and fermionic parity, as always). The y and z spin components are not conserved because of the SOC: spin-singlet and spin-triplet components mix. Furthermore, Hamiltonians with a background tunnelling term in general lack particle-hole (p-h) symmetry. In the ZBW Hamiltonian this manifests as the absence of bipartite hopping structure, since the orbitals d , f_R and f_L have triangular connectivity. The eigenvalues of the single-electron non-interacting Hamiltonian at $\Delta = 0$, which is a 6×6 matrix in the presence of SOC, are shown as a function of τ for several values of λ in Fig. 3. Generally, there is no p-h symmetry for $\tau \neq 0$, except for the special case of $\lambda = 1/2$. For $\lambda = 1/2$, the magnitudes of spin-conserving and spin-flip tunnelling become equal. One can define the transformation X that maps spin-conserving tunneling term onto the spin-flip tunneling term and vice versa:

$$\begin{aligned}
d_{\sigma}^{\dagger} &\rightarrow d_{\bar{\sigma}}, \\
c_{lk\sigma}^{\dagger} &\rightarrow i(-1)^l c_{lk\bar{\sigma}},
\end{aligned} \tag{8}$$

Here $(-1)^L = -1$ and $(-1)^R = 1$, and $\bar{\sigma}$ is spin inversion. If in addition $\phi = \pi$, then the many-body Hamiltonian H commutes with X . As we will see in the following, this leads to degeneracy of the Andreev pair qubit states. As a consequence, system properties will be anomalous in vicinity of the point $(\lambda = 1/2, \phi = \pi)$ in the parameter space. The results are symmetric with respect to $\lambda = 1/2$, thus only the interval $\lambda \in [0 : 1/2]$ needs to be considered. One can relate λ and $1 - \lambda$ through spin rotations. In particular, the case of pure spin-flip scattering ($\lambda = 1$) maps onto the case of pure normal scattering ($\lambda = 0$). The existence of special symmetry for equal spin-conserving and spin-flipping tunneling rates is expected to be generic, and does not depend on the particular choice of SOC axis and parametrization, since an analogous mapping could be derived for other forms of SOC terms.

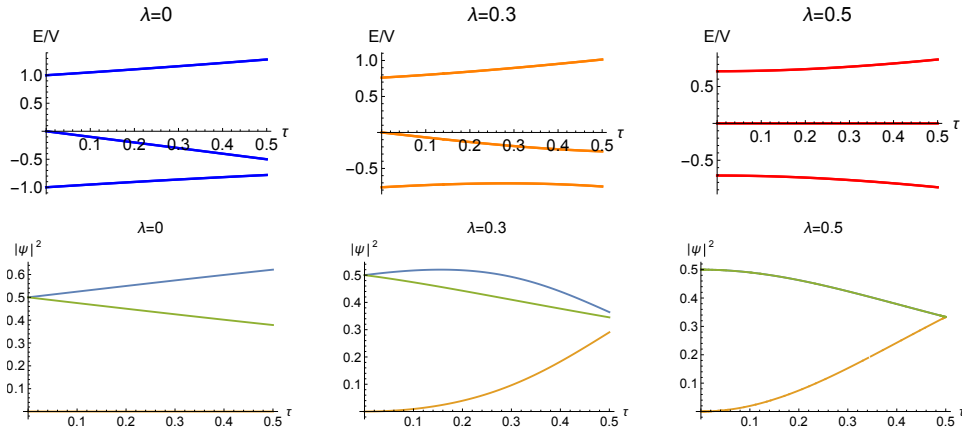


Figure 3: Top: Eigenenergies of the normal-state ($\Delta = 0$) single-electron part of the Hamiltonian for three values of the dimensionless SOC parameter λ as a function of the background tunnelling parameter $\tau = t/V$. Bottom: Corresponding probabilities for electron occupation on the QD orbital for lowest (blue), middle (orange) and highest-energy state (green).

4.2 Transition range between the ABS and YSR regimes

The $U = 2\Delta$ anomalous point is due to a quantum phase transition (level crossing) in the even-fermion-parity subspace. In the atomic limit ($V \rightarrow 0$), when U exceeds 2Δ the lowest-energy state changes from the ABS-like to the YSR-like state:

$$|\psi_{\text{ABS}}\rangle = \frac{1}{\sqrt{2}} (1 \pm d_{\uparrow}^{\dagger} d_{\downarrow}^{\dagger}) |\Phi_0\rangle \longrightarrow |\psi_{\text{YSR}}\rangle = \frac{1}{\sqrt{2}} (d_{\uparrow}^{\dagger} \gamma_{0,\downarrow}^{\dagger} - d_{\downarrow}^{\dagger} \gamma_{0,\uparrow}^{\dagger}) |\Phi_0\rangle .$$

In the two-channel AIM, the anomalous point remains at $U = 2\Delta$ in the atomic limit. The evolution with increasing coupling now also depends on the direct tunneling term $V^{(D)}$. The direct tunneling constitutes a weak link between the superconductors, hence it generates a localized quasiparticle state with an energy level inside the gap [50]. The creation of the YSR-type singlet $|\psi_{\text{YSR}}\rangle$ becomes less energetically costly, because the quasiparticle $\gamma_{0,\sigma}$ can be generated in these new states instead of being delocalized further away in the leads. The centre of the cross-over region thus shifts toward lower U .

A quantitatively adequate approximative description of the shift of the transition point can be obtained from a single-QP mode Ansatz in the YSR regime:

$$\begin{aligned} |\psi_L\rangle &= \frac{1}{\sqrt{2}} (d_{\uparrow}^{\dagger} \gamma_{L,0,\downarrow}^{\dagger} - d_{\downarrow}^{\dagger} \gamma_{L,0,\uparrow}^{\dagger}) |\Phi_0\rangle , \\ |\psi_R\rangle &= \frac{1}{\sqrt{2}} (d_{\uparrow}^{\dagger} \gamma_{R,0,\downarrow}^{\dagger} - d_{\downarrow}^{\dagger} \gamma_{R,0,\uparrow}^{\dagger}) |\Phi_0\rangle . \end{aligned}$$

Neglecting the coupling with the dot level, the "direct hopping" matrix element

$$\langle \psi_L | H_c^{(D)} | \psi_R \rangle = V^{(D)} \sin \frac{\phi}{2} ,$$

reduces the YSR state energy by:

$$E_S = \Delta - V^{(D)} \sin \frac{\phi}{2} . \quad (9)$$

As a consequence, the crossover point at finite τ shifts to

$$U^*/2 = \Delta - V^{(D)} \sin \frac{\phi}{2}. \quad (10)$$

This discussion assumes other hopping coefficients ($V^{(N)}, V^{(\text{SF})}$) to be zero. When hopping to the dot is finite, there is an opposing effect, pushing the cross-over region towards larger values of U [27]. For realistic parameters, the centre of ABS-YSR cross-over regime therefore always lies close to $U \approx 2\Delta$.

4.3 Emergence of local spin polarization

We briefly discuss how local spin polarization along the x -axis arises in a model that conserves the x -component of the total spin S_x^{total} . We define an Ansatz defined in a two-orbital space (representing impurity, d , and bath, f) composed of an impurity local singlet, an inter-orbital singlet and an inter-orbital triplet with $S_x^{\text{total}} = 0$:

$$\psi = a d_{\uparrow}^{\dagger} d_{\downarrow}^{\dagger} + \frac{b}{\sqrt{2}} (d_{\uparrow}^{\dagger} f_{\downarrow}^{\dagger} - d_{\downarrow}^{\dagger} f_{\uparrow}^{\dagger}) + \frac{c e^{i\phi}}{\sqrt{2}} (d_{\uparrow}^{\dagger} f_{\uparrow}^{\dagger} - d_{\downarrow}^{\dagger} f_{\downarrow}^{\dagger}), \quad (11)$$

with a, b, c real and satisfying normalization condition $a^2 + b^2 + c^2 = 1$. A quick calculations yields $\langle \psi | S_x^d | \psi \rangle = -bc \cos \phi$. The other spin components y and z are strictly zero. We see that the local singlet is irrelevant, while the local spin polarization is generated by the interference of inter-orbital singlet and triplet components. It is maximal for equal strength of singlet and triplet components, $b = c = 1/\sqrt{2}$, and for coefficients that are in phase, $\phi = 0$. In this case, the wavefunction factorizes as $\psi = (1/2) (d_{\uparrow}^{\dagger} - d_{\downarrow}^{\dagger}) (c_{\uparrow}^{\dagger} + c_{\downarrow}^{\dagger})$, corresponding to two spins polarized in opposite directions along the x -axis. This simple picture provides the underlying intuition for understanding the spin polarization of subgap states due to a combination of singlet and triplet YSR components with an appropriate phase relation.

5 Results

To obtain a qualitative picture of the general behaviour in the typical operating range, we now perform a study using the computationally inexpensive ZBW approach, complemented by heuristic interpretations of key observations (Secs. 5.1 to 5.5). Later, we validate these results using the NRG calculations (Sec. 5.6).

5.1 Local-moment fraction

The character of the subgap states can be most directly quantified through the ‘‘local-moment fraction’’, i.e., the probability of single-electron occupancy on the quantum dot, $P_1 = \langle n - 2n_{\uparrow} n_{\downarrow} \rangle$. From the perspective of the variational Ansatz, this corresponds to contributions from $|\psi_L\rangle$ and $|\psi_R\rangle$ (and their spin-1 equivalents). P_1 evolves from 0 in the deep ABS limit to 1 in the deep YSR limit; the change is sudden in the atomic limit ($V \rightarrow 0$), but becomes a smooth crossover for finite V . The crossover region is narrower for the excited state than for the ground state, but generally they are quite similar, see Fig. 4a,b. This generalizes the findings from Ref. [27] which focused on the ground state G in the case of a single superconductor, which corresponds to the $\phi \rightarrow 0$ limit of the present work. For $\phi = 0$, the excited state E merges with the continuum on the YSR side (see Fig. 6 in Ref. [27], as well as Fig. 7a in this work). This is a peculiarity of the $\phi = 0$ case that maps onto a single-channel Hamiltonian. For a general

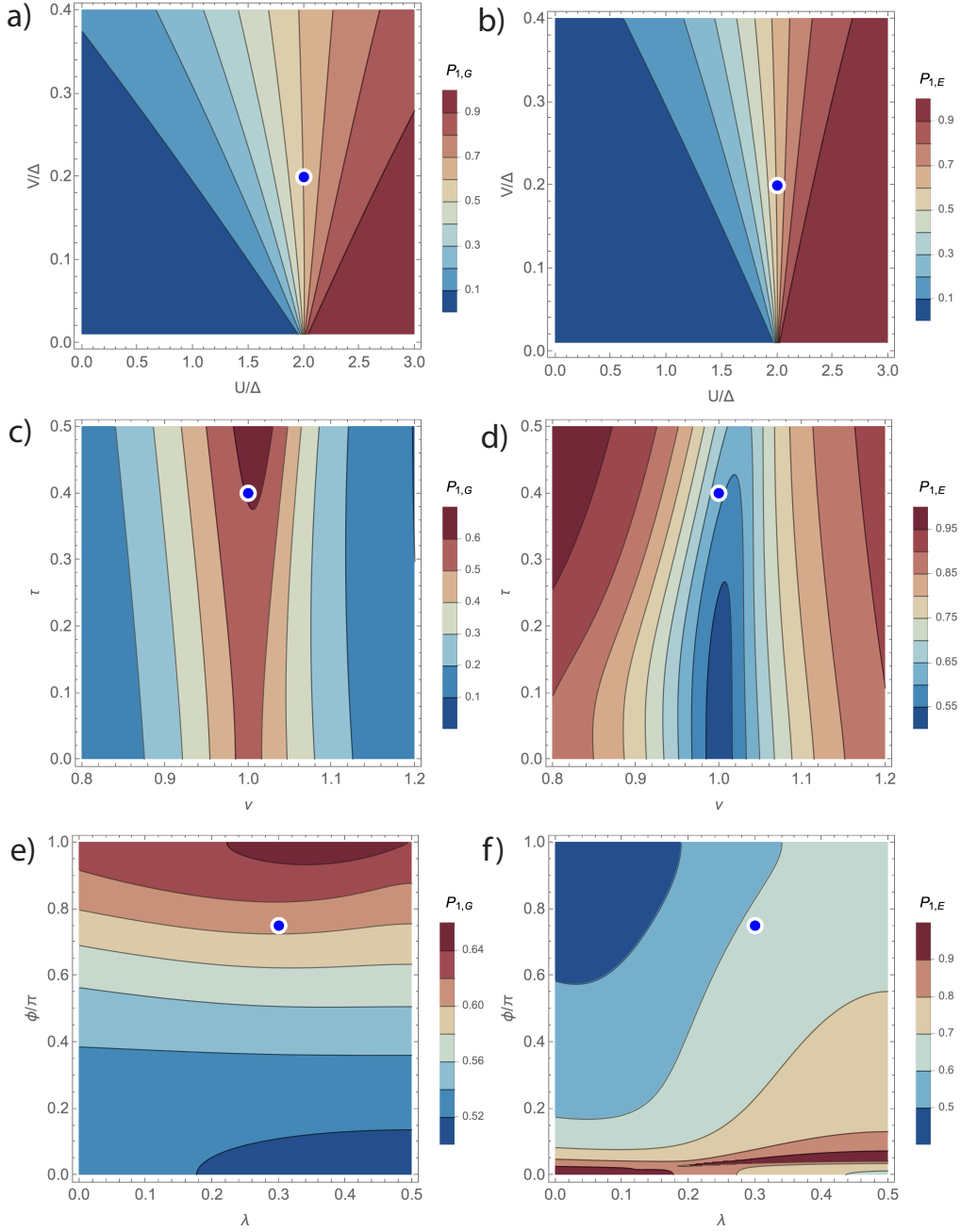


Figure 4: Local-moment fraction, i.e., the probability of single-electron occupancy on the quantum dot, $P_1 = \langle n - 2n_\uparrow n_\downarrow \rangle$, in ground (G) and excited (E) subgap states; ZBW results. (a,b) Dependence on the electron–electron repulsion U and the hybridization V . (c,d) Dependence on the displacement from half-filling, ν , and the relative strength of background tunnelling through high-energy orbitals, τ . (e,f) Dependence on the strength of spin-orbit coupling, λ , and the phase bias ϕ . Reference parameter values (Sec. 2.1) are indicated by the blue markers.

phase difference ϕ not too close to 0, there exist two subgap states for all values of U and V , including in the YSR regime [25].

The lines of constant P_1 in the (U, V) plane are almost linear (Fig. 4a,b). For low V , this follows from the variational equations (Appendix A.1) that describe linear mixing between the ABS and YSR terms, but such behaviour is seen to extend into the intermediate coupling regime, too. This scaling is, however, specific to P_1 ; other quantities tend to exhibit more complex dependencies, as will become clear in the following. We also note that the $P_1 = 0.5$ curve, which may be considered as the centre of the cross-over region, has a slight negative slope in the (U, V) plane. This is in line with the observations made in Sec. 4.2.

The dependence in the (ν, τ) plane is strikingly different for the ground and the excited state, see Fig. 4c,d. The ground state G has maximal P_1 when ν is tuned near half filling, $\nu = 1$, and it grows slightly with increasing τ . The first observation is naturally expected, since it directly results from the behaviour of the YSR singlets for large U , where ν very directly tunes the average occupancy of the impurity orbital. The weak dependence on τ is only a small correction to this general trend; in the ZBW picture, it arises because the weight of the intermediate-energy non-interacting wavefunction on the QD orbital increases with increasing τ (see also Fig. 3, bottom panels, orange lines).

Quite surprisingly, however, the local-moment fraction of the excited state E actually increases away from $\nu = 1$, see Fig. 4d. This can be understood from the requirement that the two subgap states remain orthogonal to each other. On the $\nu < 1$ side, as the ground states becomes increasingly of pure $|0\rangle$ character with decreasing ν , at the detriment of the $|1\rangle$ and $|2\rangle$ components, the lowest energy excited states maintaining orthogonality will need to have a sizeable $|1\rangle$ component, since the $|2\rangle$ part is too high in energy due to the relatively large value of the electron-electron repulsion U . Clearly, this behaviour is specific to the singular $U \sim 2\Delta$ cross-over region in vicinity of $\nu = 1$; it is not relevant for low U (where the two orthogonal states away from $\nu = 1$ are simply of $|0\rangle$ and $|2\rangle$ type, respectively, and $|1\rangle$ is merely a small interaction-induced correction), nor for high U (where the two subgap states are both YSR states with well defined local moment that is screened by two different linear combinations of Bogoliubov quasiparticles from the superconducting leads, as long as ϕ is not too close to 0 [25, 51]). Fig. 4d is a clear example of states in the crossover regime possessing unconventional properties, with the excited state displaying them most prominently.

Regarding the remaining parameters from the set, the SOC λ and the phase ϕ , for the ground state we find only a small variation of order 10% across the full range of ϕ and a tiny dependence on λ , see Fig. 4e. For the excited state, we find moderate dependence on λ and ϕ , except for the region of very small ϕ , see Fig. 4f: this is where the excited state would enter the continuum in the full model, while in the ZBW approximation it mixes with a discrete state that has the character of a doublet state with an unbound Bogoliubov quasiparticle in the superconductor. This results in a rapid variation and anomalous behaviour (here for $\phi/\pi \lesssim 0.1$) that will also be visible in other quantities presented in the following. Since the focus of this work is in generic ϕ , we will not analyse these peculiarities of the small ϕ range.

We note the opposite trend in P_1 for G and E states as regards their ϕ dependence, respectively increasing and decreasing, compare Fig. 4e and 4f. This can be explained by the opposite dispersion (energy vs. bias ϕ) of the two states: G increases with ϕ moving away from $\phi = 0$, while E decreases, see Fig. 2. Generally speaking, the vicinity to the continuum of excited states (which are essentially the doublet states with a decoupled Bogoliubov quasiparticle) tends to increase the single-occupancy component.

5.2 Magnetic response

Since subgap states host local moment, they exhibit magnetic response. For $\phi \neq 0, \pi$, and in the simultaneous presence of spin-orbit coupling and background tunnelling, the states are

spin-polarized in the absence of external magnetic field. The polarization occurs for essentially the same reasons as for the doublet states in the odd-parity subspace in Andreev spin qubit (ASQ) devices [5]. The YSR components of states G and E simply inherit these properties.

The spin polarization $\langle S_x \rangle$ of G and E states points in the opposite directions, see Fig. 5a,b. We plot the results in the (λ, ϕ) plane, as these two parameters determine the magnitude of the polarization. The odd-parity doublets in ASQs form degenerate Kramers pairs, unless all conditions for the spin splitting are present [35, 37]; spin splitting and spin polarization occur concurrently. The even-parity states are in general non-degenerate, however $\langle S_x \rangle \neq 0$ only in the presence of the specified three conditions. Because of the "pre-existing energy splitting", the effective SOC field B_{SOC} is not the same for the G and E states, see Fig. 5c,d. This quantity is extracted by applying a weak probe field along the transverse z direction and observing the change of direction of the spin polarization, which gives

$$B_{\text{SOC}} = \frac{\langle S_x \rangle}{\langle S_z \rangle} B_z. \quad (12)$$

The spin polarization grows monotonously with λ , see Fig. 5a,b. For the G state, the splitting is largest for intermediate values of ϕ close to $\pi/2$ (where time-reversal symmetry breaking is strongest) and it shifts toward $\phi = \pi$ as λ increases. At the special point $\phi = \pi$, $\lambda = 1/2$ the variation is singular, with a direction-dependent limiting value of the spin-polarization, i.e., the high-symmetry point behaves as a branch-point singularity.² For the E state, the trend as regards the ϕ -dependence is, however, the opposite as for the G state: the maximum value moves from $\phi \sim \pi/2$ towards $\phi = 0$ as λ increases.

Interestingly, the trends seen in $\langle S_x \rangle$ are not fully reflected in the behaviour of the effective SOC field. For the G state, the general trends in $\langle S_x \rangle$ and B_{SOC} are similar. For the E state, the peak in B_{SOC} as a function of ϕ moves toward $\phi = \pi$ with increasing λ , in distinction to the variation of $\langle S_x \rangle$. One should note that the spin polarization depends on two factors, the size of the effective field, as shown in Fig. 5c,d, but also on P_1 , on which we remarked an opposite ϕ dependence for G and E (see Fig. 4e,f). This P_1 effect is strong enough to control the ϕ -dependence of $\langle S_x \rangle$ as well.

For $\lambda \neq 0$, sub-gap states acquire an admixture of high-spin components, predominantly the YSR triplet, Eqs. (7), corresponding to a state in which the local moment on the QD aligns with the Bogoliubov quasiparticle spin. This is quantified through $\langle S_{\text{total}}^2 \rangle$, which vanishes for spin singlets. Fig. 5e,f reveal that the high-spin part develops with increasing λ , as expected, with weak dependence on ϕ . The largest admixture of the YSR triplet is found for the state E at low values of ϕ . This is expected, since this state is closest to the Bogoliubov continuum, where the YSR triplets are submerged in the absence of SOC. We again observe singular behaviour in vicinity of $\lambda = 1/2$, $\phi = \pi$.

5.3 Pairing properties

We now focus on the $|0\rangle$ and $|2\rangle$ components associated with proximitized superconductivity. The lack of p-h symmetry for $\tau \neq 0$, $\lambda \neq 1/2$ implies nonequal weights of $|0\rangle$ and $|2\rangle$ parts at the nominal half-filling point $\nu = 1$. Fig. 6a,b shows the (U, V) dependence of the probabilities for zero and double occupancy, P_0 and P_2 , in the state G . Both monotonically decrease with increasing U , but not at equal rates, creating imbalance between the two components. The excited state E shows the opposite pattern of P_0 and P_2 evolution, so that $P_{0,E} \sim P_{2,G}$ and $P_{2,E} \sim P_{0,G}$ (not shown). The occupancies, $\langle n \rangle = P_1 + 2P_2$, for both states deviate from 1 at the nominal half-filling point $\nu = 1$, see the case of $\langle n \rangle_G$ in Fig. 6c, but so that $\langle n \rangle_G + \langle n \rangle_E \sim 2$ to a good approximation (yet not exactly).

²The singular structure in the results is not specific to ZBW, but is also present in NRG.

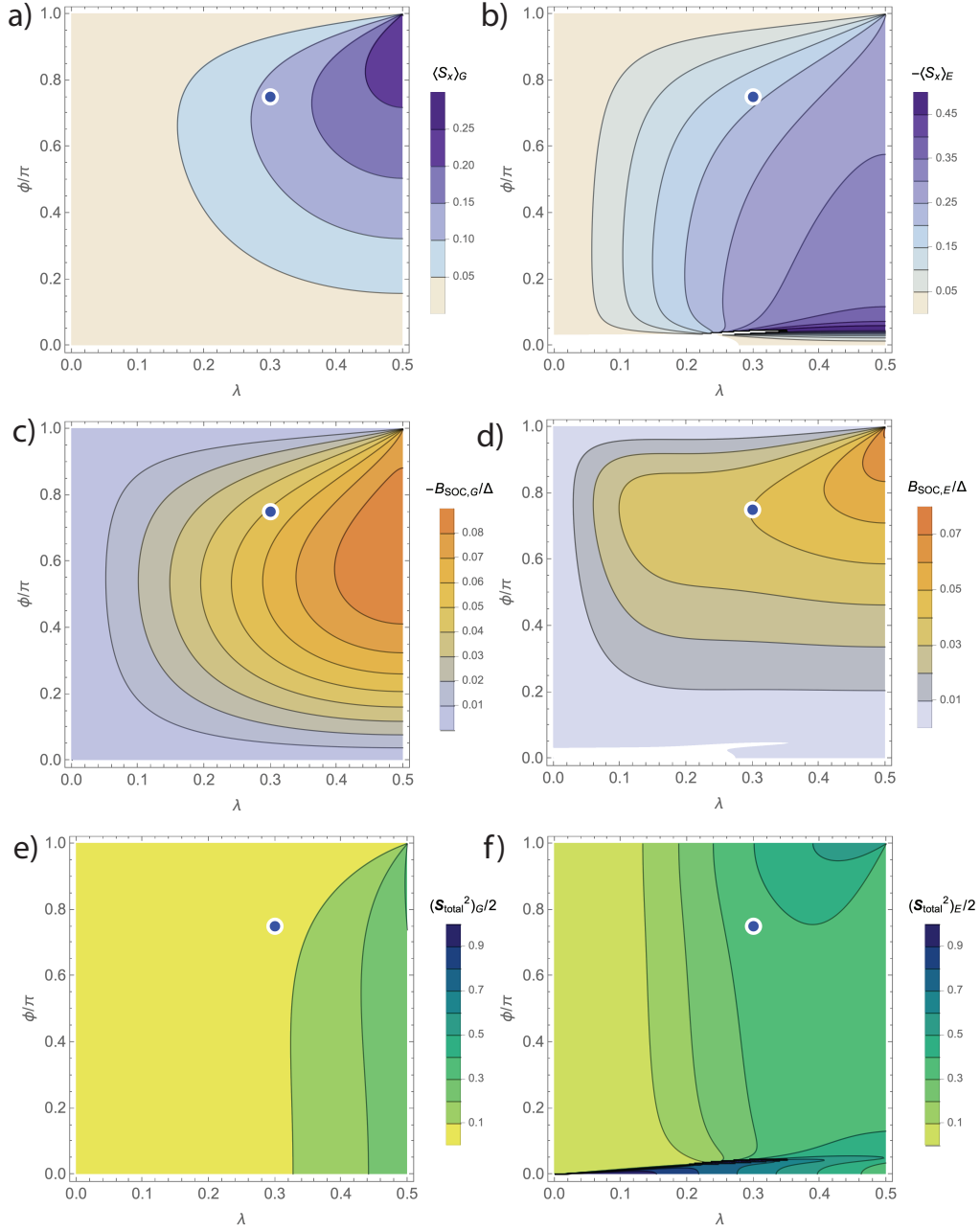


Figure 5: Magnetic properties of the subgap states as a function of the SOC strength λ and the phase bias ϕ ; ZBW results. (a,b) Spin polarization along the SOC axis (x); note the difference in signs. (c,d) Strength of the SOC effective magnetic field. (e,f) Size of the YSR spin-triplet component quantified by $\langle S_{\text{total}}^2 \rangle$.

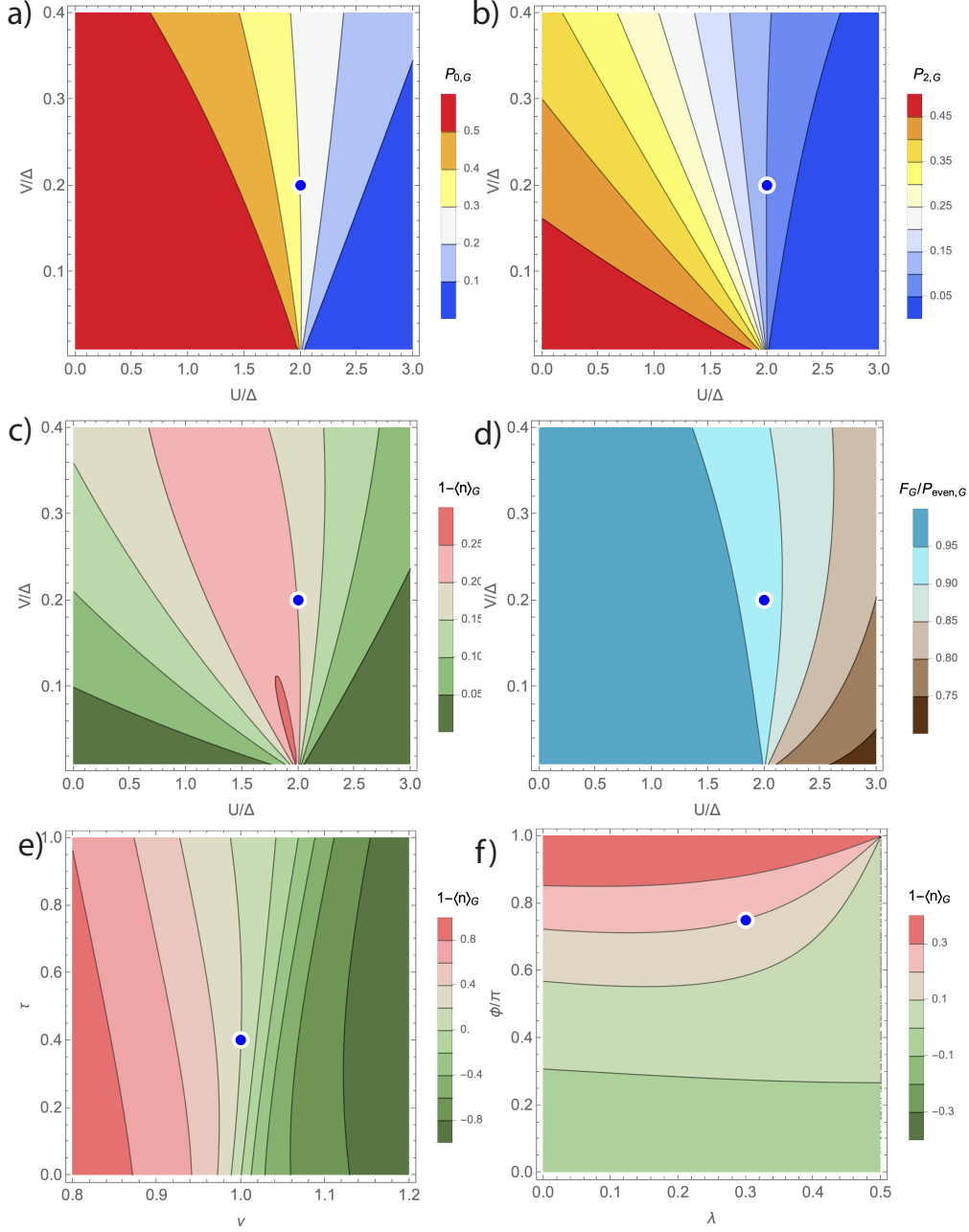


Figure 6: Pairing properties of the state G; ZBW results. (a,b) Probability of zero occupancy, P_0 , and double occupancy, P_2 , as a function of repulsion U and hybridization V . (c) Deviation from half-filling that results from these P_0 and P_2 . (d) Overlap with the conventional ABS ground-state wavefunction $\psi = 1/\sqrt{2}(e^{i\phi/4}\langle 0 \rangle + e^{-i\phi/4}\langle 2 \rangle)$, normalized by the probability of even occupancy $P_e = P_0 + P_2$. (e,f) Deviation from half-filling vs. ν and τ , and vs. λ and ϕ .

In the absence of background tunnelling and SOC, the ground-state ABS wavefunction for low U has the form

$$|\psi\rangle_G = \frac{1}{\sqrt{2}} (e^{i\phi/4} |0\rangle + e^{-i\phi/4} |2\rangle). \quad (13)$$

We can quantify the departure from this form by computing the expectation value of the projector to this state, $F = \langle P_\psi \rangle$. We furthermore take into account the emergence of single-electron component for finite U by rescaling this quantity by $P_{\text{even}} = P_0 + P_2$. We present a plot of F/P_{even} in Fig. 6d for state G (the case of state E is similar). This quantity has a value not too far from 1 in a significant part of the (U, V) plane, and even at $U \sim 2\Delta$ we still find $F/P_{\text{even}} \approx 0.9$. This shows that despite the complex (U, V) dependencies of various quantities at low V , and despite the lack of p-h symmetry, the nature of the state in the $|0\rangle, |2\rangle$ subspace (i.e., disregarding the YSR admixture) is still essentially that of an ABS to a reasonable degree of approximation for much of the $U \lesssim 2\Delta$ range.

The line where $\langle n \rangle_G = 1$ remains parametrically close to $\nu = 1$, see Fig. 6e showing the deviation from 1 in the (ν, τ) plane. This deviation depends significantly on the phase-bias ϕ and somewhat more weakly on λ , see Fig. 6f. In particular, the system can be tuned to half filling along a line in the (λ, ϕ) plane. For $\lambda = 1/2$, the system becomes p-h symmetric. For λ close to $1/2$, the deviation develops a singular structure: in most of the ϕ range it remains close to 0, but then increases suddenly as $\phi \rightarrow \pi$.

5.4 Energy separation

Before addressing the energy separation between the states G and E, we first need to establish when both states actually exist within the gap. In the limit $\phi \rightarrow 0$, this is the case only in the ABS regime. The excited state merges with the continuum of Bogoliubov states close to $U \sim 2\Delta$, see for example Fig. 6b in Ref. [27]. For $\phi = 0$, only a single linear combination of Bogoliubov states from the superconductors couples to the impurity orbital, while a second scattering channel emerges only at finite ϕ .³ The region where the E state does not exist is rather small for generic parameters and confined to low values of ϕ in the $U > 2\Delta$ range. For the reference values used in this work, it is restricted to $\phi/\pi \lesssim 0.05$, see Fig. 7a (white region enclosed within the red curve). The same plot also reveals that the E state remains rather close to the gap edge for $U \gtrsim 2\Delta$.

In Fig. 7b,c,d we show the energy splitting $E_E - E_G$ along three cuts in the parameter space: (U, V) plane, (ν, τ) plane, and (λ, ϕ) plane for panels b,c,d, respectively. The splitting monotonously grows with V , with the largest splitting for a given value of V occurring for $U \sim 2\Delta$ (see panel b): this directly reflects that fact that this region is controlled by the singularity associated with increased state degeneracy [27], with two ABS states being resonant with the divergently dense Bogoliubov states at the band edge, a feature that is captured at qualitative level even within the ZBW approximation [54]. The splitting grows as one moves away from half filling ($\nu = 1$), since detuning enhances the energy difference beyond that induced by the proximity effect alone by altering the relative weights of the $|0\rangle$ and $|2\rangle$ components (see panel c). At the chosen reference point, the background tunnelling ratio τ has little effect on the energetics. Finally, the plot in panel d directly reveals the approach to the degeneracy point $E_G = E_E$ at $\lambda = 1/2, \phi = \pi$ due to the enhanced symmetry.

³An arbitrary number of SC leads can be integrated out to define a single matrix-valued (Nambu) hybridization function that can be mapped to a single Wilson chain [52, 53]. In this sense, the SC-AIM is effectively a single-bath quantum impurity problem. Nevertheless, for a finite phase bias, the existence of the second scattering channel [25] is encoded in the out-of-diagonal matrix elements being reduced compared to the $\phi = 0$ limit by a factor of $\cos(\phi/2)$. In addition, in the presence of background tunnelling τ , the hybridization matrix encodes sub-gap δ -peak contributions corresponding to additional in-gap states [50].

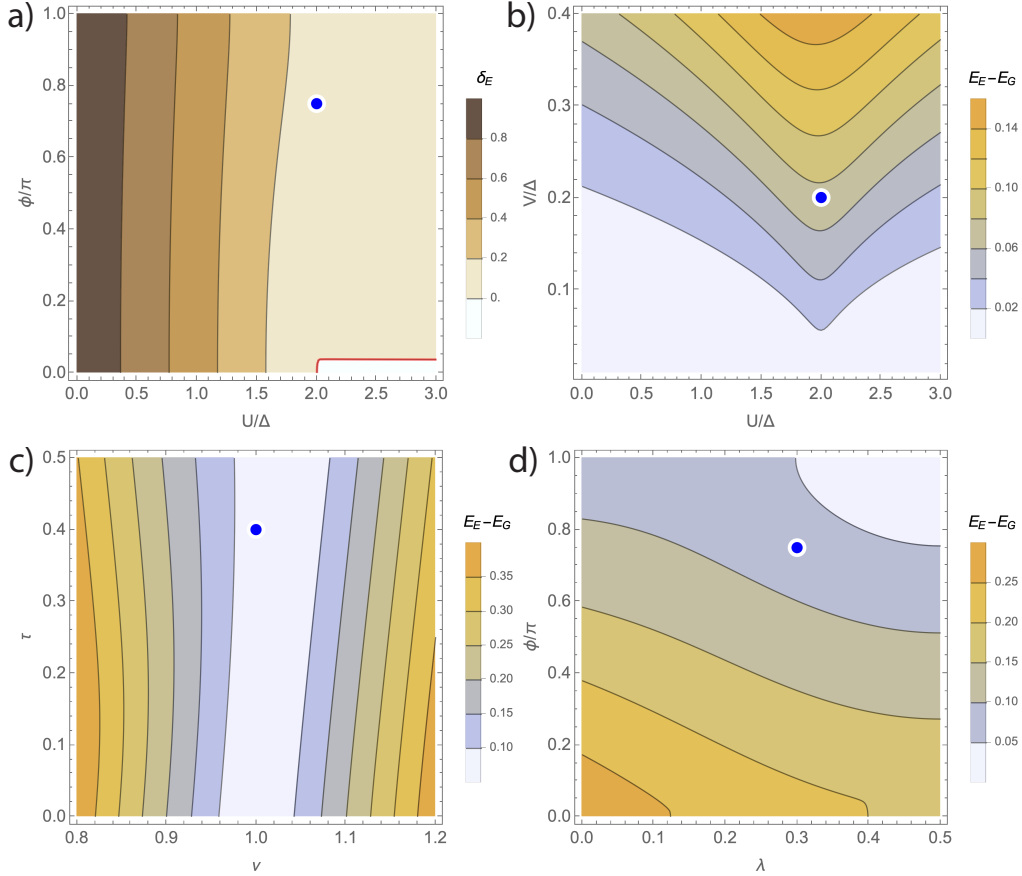


Figure 7: Energies of the subgap states; ZBW results. (a) Binding energy of the excited subgap state, δ_E , i.e., its position below the continuum of Bogoliubov excitation. Negative value indicates that the excited state is absorbed in the continuum (corresponding to a level crossing in ZBW approximation). The red curve indicates the locus of $\delta_E = 0$. (b,c,d) Energy splitting between G and E states as a function of different parameter pairs.

5.5 Transition matrix elements

Transitions between the subgap states G and E have particular parameter dependencies for the three main control channels (charge, spin and current) due to the changing nature of the states themselves. Fig. 8a shows the expected trend towards insensitivity to gate-potential driven transitions as the system moves from the ABS to the YSR regime; this plot simply reflects the growth of single electron occupancy quantified by $P_{1,G}$ and $P_{1,E}$ and thus strongly resembles Fig. 4a,b. Correspondingly, Fig. 8c shows how spin transitions become possible for strong enough interaction U . This crossover in spin channel is more abrupt than the one in the charge channel. This can be ascribed to the properties of the state E: the expectation value $\langle S_x \rangle_E$ shows a similar threshold behaviour as a function of U , whereas $\langle S_x \rangle_G$ shows a smoother evolution (plots not shown). We note again that in the absence of SOC, background tunnelling, or finite ϕ , this matrix element would be zero. Fig. 8e shows how for inductive transitions (flux driving [14, 55–57]) the evolution in the (U, V) plane reflects the dispersion of states which becomes larger as V increases, especially in the $U \approx 2\Delta$ range; since strong dispersion also implies large level separation, this plot resembles that of $E_E - E_G$ in Fig. 7b.

Fig. 8b,d,f reveal that charge transitions are strong for intermediate values of $\phi \sim \pi/2$ with only a weak λ -dependence that slightly favours small SOC, magnetic transitions are favoured by strong SOC and phase bias close to π , while inductive transitions are favoured by weaker SOC and phase bias close to π . It should be noted that for $\phi = \pi$ the charge transitions are forbidden. This is because $|G\rangle$ has no $|2\rangle$ component, while $|E\rangle$ has no $|0\rangle$ component in this limit, if $\tau \neq 0$. At $\phi = \pi$, the relative strength of spin and inductive transitions depends on λ . Similarly, one can find parameter choices where either spin or inductive transitions become negligible. Finally, there are clearly regimes where all three couplings are large. These tuning capabilities might be of interest, for example, for applications in quantum transduction.

5.6 NRG validation

While NRG calculations for the full model with SOC and two SC leads with a phase bias are numerically very costly, we have been able to perform a systematic study that supports the qualitative correctness of the results obtained using the ZBW approximation in the preceding subsections. Because the superconductors are now described using continuum Hamiltonians, the hybridization and background tunnelling terms are defined differently: the hybridization will be expressed in terms of the total hybridisation strength $\Gamma = 2\pi\rho V^2$, where ρ is the normal-state density of states of each lead, while the background tunnelling will be quantified through τ' defined as $V^{(D)} = \tau'\sqrt{\Gamma D}$, where D is the half-bandwidth of the bath. Other parameters are defined as before and we used the same values as in the reference parameter set for the ZBW approximation in the earlier sections.

In Fig. 9 we plot the U -dependence of key quantities. This calculation is performed for intermediately strong coupling $\Gamma = 0.1\Delta$; this value is typical of hybrid nanowire devices [58]. The local-moment fraction P_1 evolves from values close to 0 to values close to 1 as the system evolves from the ABS to YSR regime (panel a); as in Fig. 4(a,b) we find that the state E crosses over faster than state G. The projectors $P_{0,G}$ and $P_{2,G}$ (panel b) also generally follow the behaviour seen for the ZBW in Fig. 6(a,b). Likewise, the occupancy in state G is suppressed for $U \lesssim 2\Delta$, with a local minimum at $U \approx 1.5\Delta$ (panel c), similar to what is seen in Fig. 6(c); the state E shows increased local occupancy in this range. The spin polarization (panel d) increases for $U \sim 2\Delta$ and it peaks somewhere in the $U > 2\Delta$ range; this is particularly pronounced for the state E. The same behaviour is found in the ZBW model (results not shown). From the energy positions with respect to the ground state (panel e) we read off that the maximum level separation occurs for $U \gtrsim 2\Delta$, in agreement with Fig. 7(b). Finally, the matrix elements (panel f) show the same trends as the ZBW prediction in Fig. 8(a,c,e).

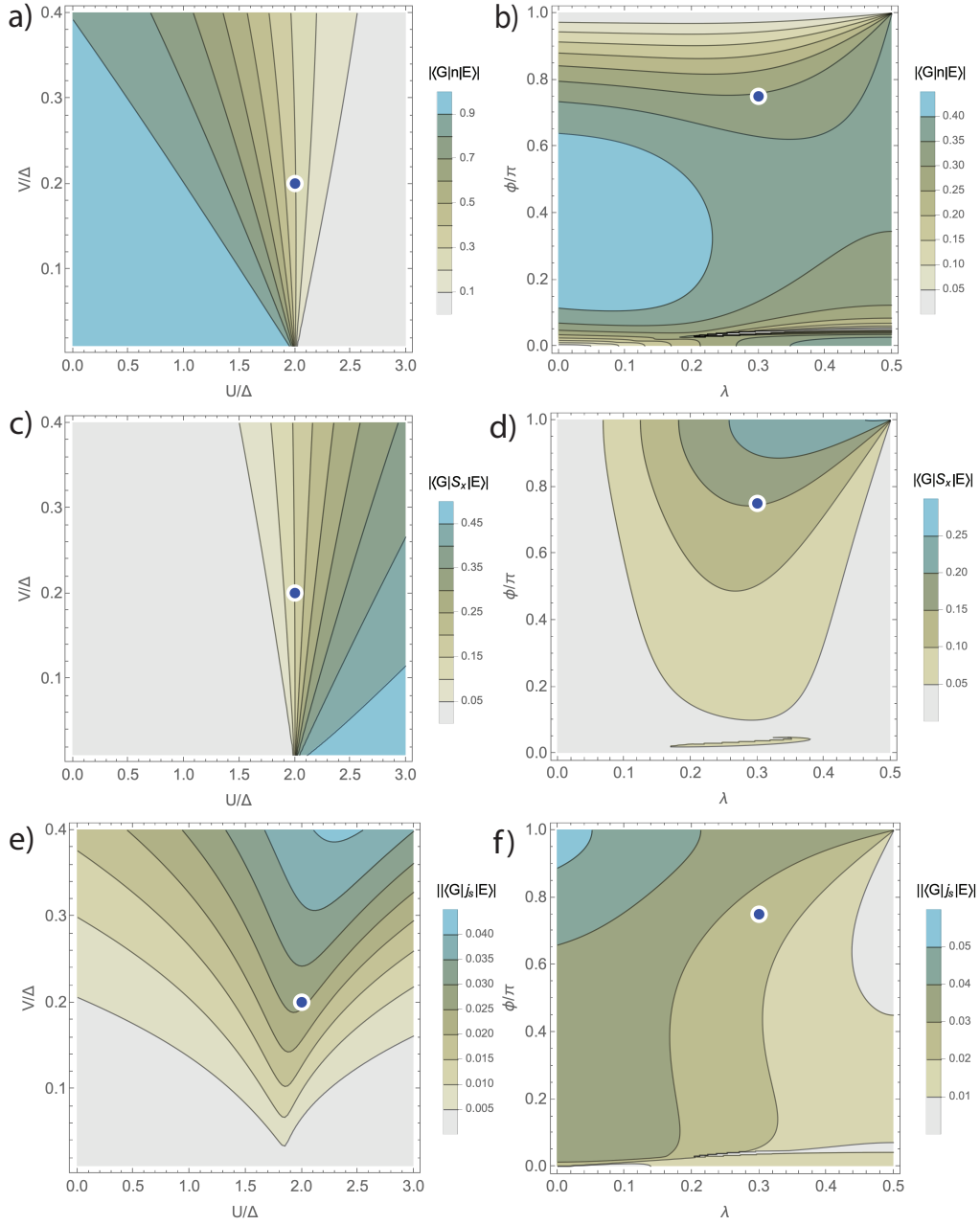


Figure 8: Matrix elements for transitions between states G and E for the QD charge operator n , the QD spin operator S_x , and the Josephson supercurrent, here defined as the dimensionless operator quantity $j_s = \langle \partial H / \partial \phi \rangle / \Delta$; ZBW results. (a,c,e) Dependence on the repulsion U and the hybridization V . (b,d,f) Dependence on the SOC parameter λ and the phase bias ϕ .

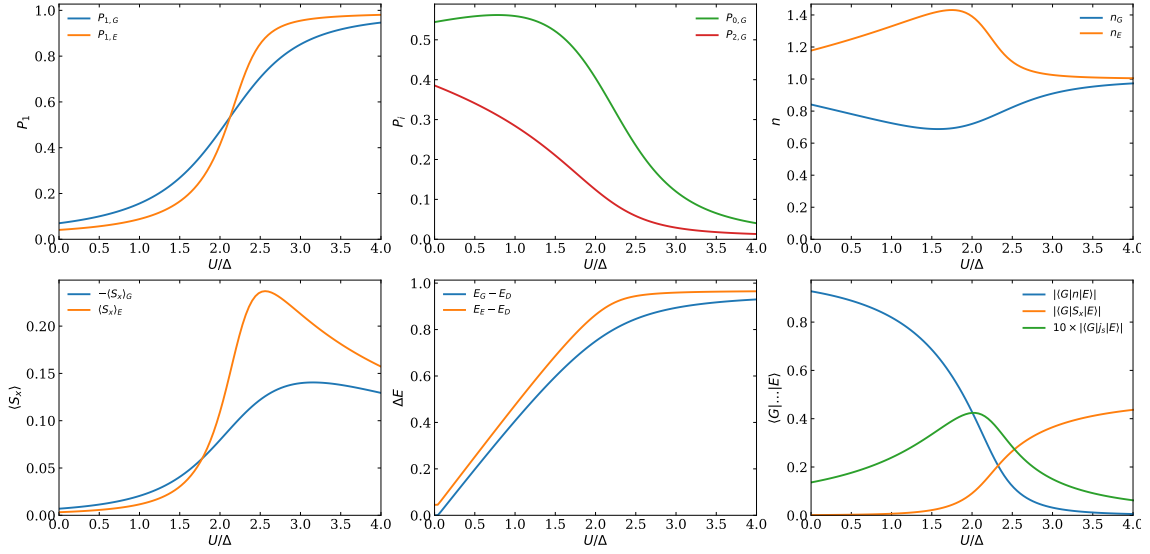


Figure 9: NRG results: U -dependence of key properties for $\Gamma/\Delta = 0.1$, $\nu = 1$, $\phi = 0.75\pi$, $\lambda = 0.3$, and $\tau' = 3$.

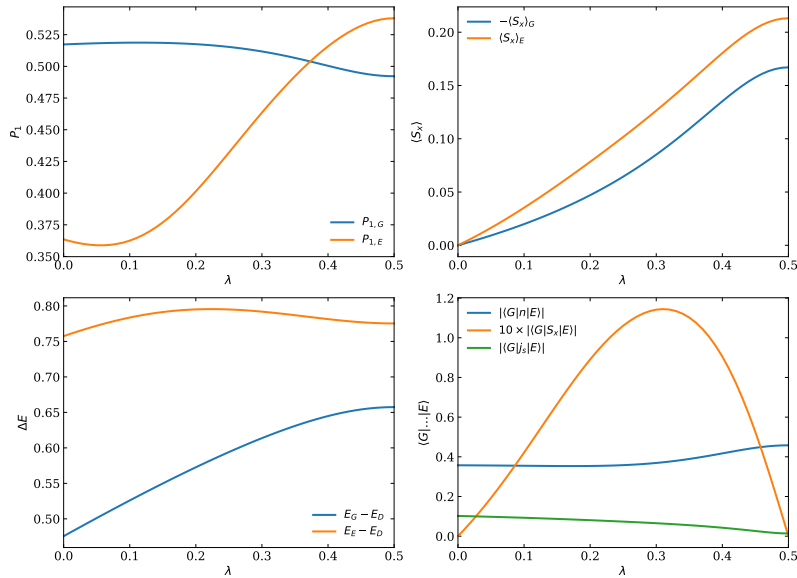


Figure 10: NRG results: λ -dependence for $U/\Delta = 2$, $\Gamma/\Delta = 0.2$, $\nu = 1$, $\phi = 0.75\pi$, and $\tau' = 3$.

In Figs. 10 we address the SOC dependence. We find the same trends as in ZBW, compare with Figs. 5(a,b), 7(d) and 8(b,d,f), down to certain details, for example $|\langle G|n|e\rangle|$ first being relatively flat, and then increasing, which is indeed the behaviour seen in ZBW model in the same range of ϕ .

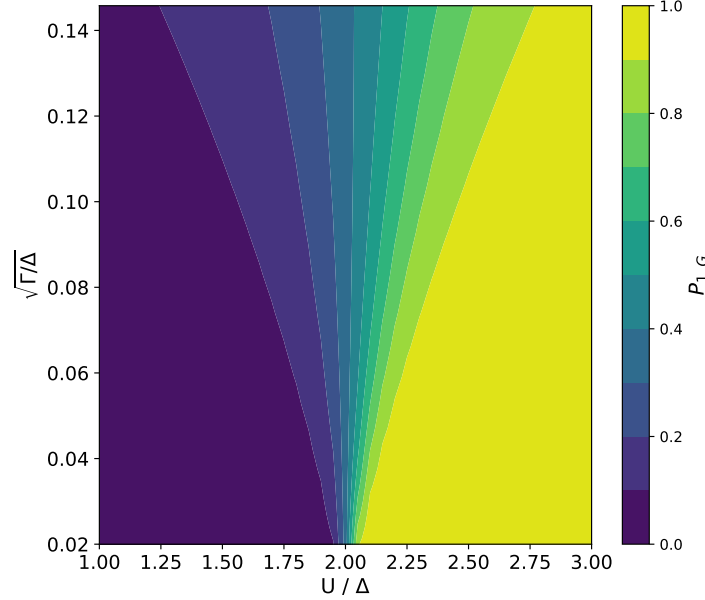


Figure 11: NRG results: local-moment fraction $P_{1,G}$ in the $(U, \sqrt{\Gamma})$ plane at half-filling, $\nu = 1$, and no SOC, $\lambda = 0$. The single-channel case is shown, corresponding to $\tau, \phi = 0$. Lines of constant $P_{1,G}$ are almost linear in the range shown, qualitatively matching the ZBW results (see Fig. 5).

In Fig. 11 we show $P_{1,G}$ in the (U, V) plane for the single-channel ($\phi, \tau = 0$) case with no SOC, $\lambda = 0$. By comparing the results with Fig. 4, we conclude that the qualitative behaviour in the (U, V) plane can be correctly captured by the ZBW approximation. Most features from Fig. 11 extend to the general two-channel case.

In Fig. 12 we plot phase-bias dependences for a range of λ that also includes some values close to $\lambda^* = 1/2$. Particularly noteworthy are the results for the occupancy, n_G , whose drop to small values becomes particularly sharp as $\lambda \rightarrow \lambda^*$. This explains anomalies seen in all other quantities, for instance the drop in spin polarization and matrix element for the charge operator.

Finally, we return to the gate-voltage dependence of the local-moment fraction P_1 , where we remarked unusual behaviour for the state E. We systematically investigated this quantity for a range of U/Δ ratios, see Fig. 13. The results show that in a range of U/Δ spanning the ABS-YSR crossover region this quantity has a minimum value in vicinity of $\nu = 1$, where a maximum value is generally expected for low-energy states. This minimum becomes well developed with increasing U as soon as P_1 starts to become appreciable, for $U/\Delta \sim 1$. It fades away deeper in the YSR regime; it is hardly visible at $U/\Delta \sim 5$. This is thus indeed a particularity of the cross-over region.

Taken together, these results establish that the ZBW correctly reproduces all key features of the ABS-YSR crossover at the qualitative level. This is due to charge physics and level occupancies being controlled by the high energy scales and local effects, which are captured adequately even by truncated-basis models. Nevertheless, we note that the use of the NRG is essential both in obtaining quantitatively correct results, and in capturing all qualitative features of the model. Since the continuum effects are not included, phenomena like the anoma-

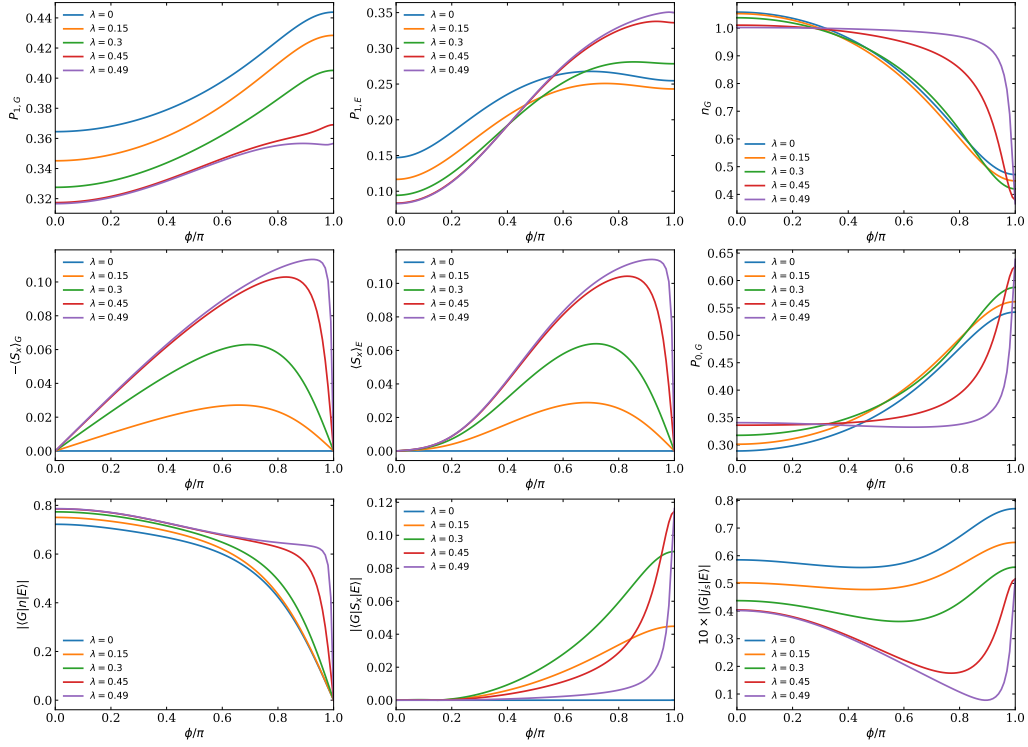


Figure 12: NRG results: ϕ -dependence for $U/\Delta = 2$, $\Gamma/\Delta = 0.1$, $\nu = 1$, $\lambda = 0.3$, and $\tau' = 3$.

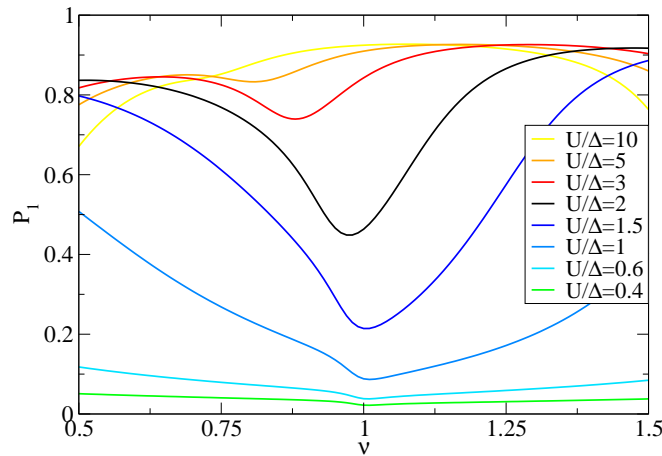


Figure 13: NRG results: ν -dependence of the local-moment fraction P_1 in the excited state E for a range of U/Δ , showing a *minimum* for $\nu \sim 1$ in the cross-over range. Other parameters are fixed: $\Gamma/\Delta = 0.1$, $\phi = 0.75\pi$, $\lambda = 0.3$, and $\tau' = 3$.

lous $\Gamma^{2/3}$ scaling of binding energies [27] cannot be produced within the ZBW framework. In such cases, either NRG or a variational calculation (see Appendix A, [27]) is required.

6 Discussion: design implications

The results presented in the previous section have some clear design implications. In particular, for qubits optimized for charge coupling with minimal magnetic sensitivity, it is crucial to remain in the ABS-dominated regime with $U \ll 2\Delta$, with small or moderate λ . For devices aiming to exploit spin-selective transitions, the crossover regime $U \approx 2\Delta$ with moderate λ and τ is optimal. In fact, device platforms that are suitable for building ASQs would also be appropriate for these applications. It should be noted, however, that in this parameter regime, the overall ground state of the system is in the odd-parity sector (spin-doublet). A long parity lifetime is thus required.

7 Conclusion

We have studied the superconducting Anderson impurity model for an interacting quantum dot Josephson junction with spin-orbit coupling. We uncovered some noteworthy properties: 1) mixing of ABS and YSR leads to properties that are not typical for pure charge qubit states, because the even-parity states carry local moments; 2) in the presence of SOC, both subgap states are spin polarized in the absence of magnetic field; 3) matrix elements are large in charge (capacitive), spin (magnetic), and current (inductive) channels, with the possibility of tuning the relative values.

An important next step is to extend this analysis to the multi-orbital junctions with several "active" levels, which are directly relevant for devices exhibiting several ABS pairs in the relevant frequency window.

Acknowledgments

Funding information We acknowledge the support of the Slovenian Research and Innovation Agency (ARIS) under P1-0416 and J1-3008, and discussions with Don Rolih and Peter Zalom, in particular on the topic of symmetry properties of impurity Hamiltonians.

A Variational approach

A.1 Variational equations

The Bogoliubov quasiparticle operators in the Ansatz from Sec. 3.3 are defined as

$$\begin{aligned}\gamma_{lk\uparrow} &= u_{lk}c_{lk\uparrow} - v_{lk}c_{l-k\downarrow}^\dagger \\ \gamma_{l-k\downarrow}^\dagger &= v_{lk}^*c_{lk\uparrow} + u_{lk}^*c_{l-k\downarrow}^\dagger,\end{aligned}$$

with symmetric phase factors in the BCS coherence factors (to simplify subsequent expressions):

$$u_{lk} = e^{i\phi_l/2} \sqrt{\frac{1}{2} \left(1 + \frac{\epsilon_k}{E_k}\right)},$$

$$v_{lk} = e^{-i\phi_l/2} \sqrt{\frac{1}{2} \left(1 - \frac{\epsilon_k}{E_k}\right)}.$$

Here, $E_k = \sqrt{\Delta^2 + \epsilon_k^2}$ is the dispersion of Bogoliubons. We also choose a symmetric gauge $\phi_R = -\phi_L = \phi/2$.

To make contact with our previous work on the single-channel case [27], we first consider the half-filling case ($\nu = 1$) with no direct tunneling ($\tau = 0$) and no SOC ($\lambda = 0$). In this limit, the symmetry will allow us to reduce the minimization problem to a single transcendental equation for the energy of singlet states, as in the single-channel case.

Minimization of the functional $f \equiv \langle \Psi | H | \Psi \rangle - \varepsilon \langle \Psi | \Psi \rangle$ yields the following variational equations for the singlet-state energy ε :

$$\left(\varepsilon - \frac{U}{2}\right) a^\pm = \frac{V_L^{(N)}}{\sqrt{N}} \sum_k \alpha_{Lk} (v_{Lk}^* \pm u_{Lk}^*) + \frac{V_R^{(N)}}{\sqrt{N}} \sum_k \alpha_{Rk} (v_{Rk}^* \pm u_{Rk}^*), \quad (\text{A.1})$$

$$\begin{aligned} (\varepsilon - E_{Lk}) \alpha_{Lk} &= \frac{V_L^{(N)}}{\sqrt{N}} a^+ (v_{Lk} + u_{Lk}) + \frac{V_L^{(N)}}{\sqrt{N}} a^- (v_{Lk} - u_{Lk}) \\ &+ \frac{V_L^{(N)}}{\sqrt{N}} \sum_{k'} (u_{Lk'}^* - v_{Lk'}^*) \beta_{LLkk'}^+ + \frac{V_L^{(N)}}{\sqrt{N}} \sum_{k'} (u_{Lk'}^* + v_{Lk'}^*) \beta_{LLkk'}^- \\ &+ \frac{V_R^{(N)}}{\sqrt{2N}} \sum_{k'} (u_{Rk'}^* - v_{Rk'}^*) \beta_{LRkk'}^+ + \frac{V_R^{(N)}}{\sqrt{2N}} \sum_{k'} (u_{Rk'}^* + v_{Rk'}^*) \beta_{LRkk'}^-, \end{aligned} \quad (\text{A.2})$$

$$\begin{aligned} (\varepsilon - E_{Rk}) \alpha_{Rk} &= \frac{V_R^{(N)}}{\sqrt{N}} a^+ (v_{Rk} + u_{Rk}) + \frac{V_R^{(N)}}{\sqrt{N}} a^- (v_{Rk} - u_{Rk}) \\ &+ \frac{V_R^{(N)}}{\sqrt{N}} \sum_{k'} (u_{Rk'}^* - v_{Rk'}^*) \beta_{RRkk'}^+ + \frac{V_R^{(N)}}{\sqrt{N}} \sum_{k'} (u_{Rk'}^* + v_{Rk'}^*) \beta_{RRkk'}^- \\ &+ \frac{V_L^{(N)}}{\sqrt{2N}} \sum_{k'} (u_{Lk'}^* - v_{Lk'}^*) \beta_{LRk'k}^+ + \frac{V_L^{(N)}}{\sqrt{2N}} \sum_{k'} (u_{Lk'}^* + v_{Lk'}^*) \beta_{LRk'k}^-, \end{aligned} \quad (\text{A.3})$$

$$\left(\varepsilon - \frac{U}{2} - (E_{lk} + E_{lk'})\right) \beta_{llkk'}^\pm = \frac{V_l^{(N)}}{2\sqrt{N}} \alpha_{lk} (u_{lk'} \mp v_{lk'}) + \frac{V_l^{(N)}}{2\sqrt{N}} (u_{lk} \mp v_{lk}) \alpha_{lk'}, \quad (\text{A.4})$$

$$\left(\varepsilon - \frac{U}{2} - (E_{Lk} + E_{Rk'})\right) \beta_{LRkk'}^\pm = \frac{V_R^{(N)}}{\sqrt{2N}} \alpha_{Lk} (u_{Rk'} \mp v_{Rk'}) + \frac{V_L^{(N)}}{\sqrt{2N}} (u_{Lk} \mp v_{Lk}) \alpha_{Rk'}. \quad (\text{A.5})$$

By substituting the variational coefficients a^\pm and β from Eqs. (A.1), (A.4), (A.5) we can obtain equations for α_{Lk}, α_{Rk} in the η -even and the η -odd sector. The even sector equations

are

$$[\varepsilon^+ - E(x) - (\Gamma/\pi)I_2(x, \varepsilon^+)]\alpha_L(x) = \frac{\Gamma s_L(x)}{2\pi(\varepsilon^+ - U/2)} \left(\int \alpha_L(x')s_L^*(x')dx' + \int \alpha_R(x')s_R^*(x')dx' \right) \quad (\text{A.6})$$

$$[\varepsilon^+ - E(x) - (\Gamma/\pi)I_2(x, \varepsilon^+)]\alpha_R(x) = \frac{\Gamma s_R(x)}{2\pi(\varepsilon^+ - U/2)} \left(\int \alpha_L(x')s_L^*(x')dx' + \int \alpha_R(x')s_R^*(x')dx' \right) \quad (\text{A.7})$$

Here, we switched to the continuum limit ($\varepsilon_k \rightarrow x$) notation, and assumed constant density of states $\rho = 1/2D$. We also introduced the function $s_l(x) = u_l(x) + v_l(x)$ for the even linear combination of coherence factors and

$$I_2(x, \varepsilon) = \int \frac{dx'}{\varepsilon - U/2 - (E(x) + E(x'))}$$

for the leading two-QP contribution. Finally, we defined $\Gamma = \pi\rho \left((V_L^{(N)})^2 + (V_R^{(N)})^2 \right)$. Note that in Eqs. (A.6), (A.7), we neglect other terms that come from the two-QP states. Here, these only correspond to small quantitative corrections and do not significantly affect the range of validity of the variational solution [27].

The Hamiltonian has an anti-unitary particle-hole symmetry for any value of the phase-difference ϕ , given by ΠK , where:

$$\Pi := \begin{cases} d_\sigma \rightarrow -d_{\bar{\sigma}}^\dagger \\ c_{lk\sigma} \rightarrow c_{l\bar{k}\bar{\sigma}}^\dagger \end{cases}, \quad (\text{A.8})$$

and K denotes complex conjugation. Here $\bar{\bullet}$ refers to the inversion of spin and the reflection of k with respect to the Fermi surface. Since we are considering the particular case of $\Delta_L = \Delta_R$, $V_L = V_R$, the Hamiltonian also has an anti-unitary mirror symmetry MK , where:

$$M := c_{lk\sigma} \rightarrow c_{l\bar{k}\sigma}, \quad (\text{A.9})$$

and \bar{l} mirrors the channel (e.g. $\bar{L} = R$). The particular form of MK makes use of the symmetric gauge, where conjugation is required to "swap" the values of ϕ_L and ϕ_R . Combining these two symmetries allows us to define a *unitary* transformation:

$$\eta := \begin{cases} d_\sigma \rightarrow -d_{\bar{\sigma}}^\dagger \\ c_{lk\sigma} \rightarrow c_{l\bar{k}\bar{\sigma}}^\dagger \end{cases}, \quad (\text{A.10})$$

which leaves the Hamiltonian invariant. This symmetry exists for any value of ϕ .

We find $\eta|\varphi^+\rangle = +1|\varphi^+\rangle$ and $\eta|\varphi^-\rangle = -|\varphi^-\rangle$. For other states in the Ansatz (5), one can find specific linear combinations with definite parity. For example, $|\psi^+\rangle = |\psi_L\rangle + |\psi_R\rangle$, along with the condition $\alpha_{Lk} = \alpha_{R\bar{k}}$ defines an η -even state. Similar construction gives an odd single-QP state $|\psi^-\rangle$ provided that $\alpha_{Lk} = -\alpha_{R\bar{k}}$. The same considerations apply to the two-QP states.

The functions $s_l(x)$ are even with respect to the η symmetry: $s_R(-x) = s_L(x)$. The transformation acts on the coherence factors by inverting the energy ($x \rightarrow -x$) and changing the label L to R and vice-versa. The symmetry of $s_l(x)$ -functions is a direct consequence of $v_l(x) = u_l(-x)$ and $\phi_L = -\phi_R$. In practice, the symmetry can be utilized to reduce the system to a single equation for $\alpha(x) = \alpha_L(x) + \alpha_R(-x)$:

$$[\varepsilon^+ - E(x) - (\Gamma/\pi)I_2(x, \varepsilon^+)]\alpha(x) = \frac{\Gamma}{\pi} \frac{s_L(x)}{\varepsilon^+ - U/2} \int \alpha(x')s_L^*(x')dx' \quad (\text{A.11})$$

We explicitly express $\alpha(x)$, multiply the expression with $s_L^*(x)$ and integrate with respect to x to get a transcendental equation for the energy of the even state:

$$\varepsilon^+ = U/2 + \frac{\Gamma}{\pi} \int dx \frac{1 + 2|u(x)||v(x)| \cos(\varphi/2)}{\varepsilon^+ - E(x) - (\Gamma/\pi)I_2(x, \varepsilon^+)}. \quad (\text{A.12})$$

Note the correspondence of this equation with Eq. (26) in Ref. [27], up to the $\cos(\phi/2)$ factor. This is the same factor that appears in the anomalous part of the hybridization function. It should be remarked, however, that we have made use of a different symmetry in the two works, p-h symmetry in Ref. [27] and the η -parity (p-h with reflection) in this work. From previous work we know that the equation correctly captures all spectral features in the low- Γ regime, including the anomalous $\Gamma^{2/3}$ scaling [27].

Similar procedure with $\alpha(x) = \alpha_L(x) - \alpha_R(-x)$ leads to the equation for the odd state:

$$\varepsilon^- = U/2 + \frac{\Gamma}{\pi} \int dx \frac{1 - 2|u(x)||v(x)| \cos(\varphi/2)}{\varepsilon^- - E(x) - (\Gamma/\pi)I_2(x, \varepsilon^-)}. \quad (\text{A.13})$$

The roots of these equations can be obtained numerically. In Fig. 14 we compare the variational solutions with the NRG data, finding good agreement at low to intermediate values of the hybridization strength Γ .

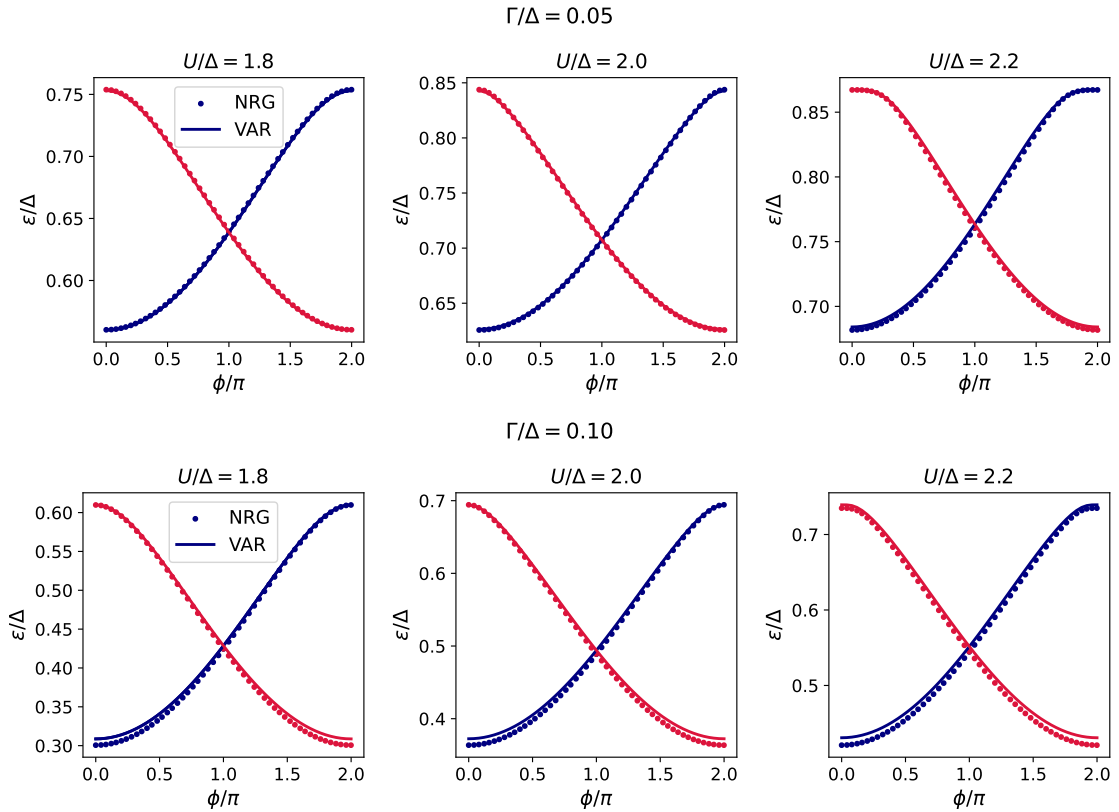


Figure 14: Variational estimates of the subgap energies for a range of Γ and U . The even (odd) variational solution is shown with a solid blue (red) line. The corresponding NRG data (dots) is shown as a reference.

A.2 Wave-function properties and crossover between regimes

The contribution of the two-QP components in the eigenenergy expressions (the I_2 terms) in Eqs. (A.12) and (A.13) takes the form of a pole-shift in the integrand and hence has a

significant quantitative role in the calculation of ε^\pm . In spite of this, due to the high energy cost of the two-QP excitations, for typical parameters the weights of the components $|\chi_{ll'}^\pm\rangle$ are orders of magnitude smaller than those of other states in the Ansatz⁴. Therefore, we can approximate the single-QP weights by the equations

$$\alpha_l^+(x) = \frac{V}{\sqrt{2N}} a^+ \frac{s_l(x)}{\varepsilon^+ - E(x) - (\Gamma/\pi)I_2(x, \varepsilon^+)}, \quad (\text{A.14})$$

$$\alpha_l^-(x) = \frac{V}{\sqrt{2N}} a^- \frac{s_l(x)}{\varepsilon^- - E(x) - (\Gamma/\pi)I_2(x, \varepsilon^-)}, \quad (\text{A.15})$$

where the contribution of two-QP states is neglected everywhere except in the factor $I_2(x, \varepsilon)$ and in the I_2 pole shift in eigenvalue equations for ε^\pm . The normalization condition is:

$$|a^\pm|^2 + 2\rho \int dx |\alpha_L^\pm(x)|^2 = 1, \quad (\text{A.16})$$

where we made use of $|\alpha_L(x)| = |\alpha_R(x)|$. Note that these correspond to occupancy probabilities, i.e., $P_1 = 2\rho \int dx |\alpha_L^\pm(x)|^2$ and $P_0 + P_2 = |a^\pm|^2$. One possible application of these analytical expressions is thus to determine the composition of the wavefunction. As an example, one can define the crossover between the ABS and YSR regimes by considering the leading contribution in the wave function. The crossover line is defined by

$$|a_1|^2 = |a|^2 = 2\rho \int dx |\alpha_L^\pm(x)|^2, \quad (\text{A.17})$$

which leads to

$$1 = \frac{\Gamma}{\pi} \int dx \frac{|s_L(x)|^2}{(\varepsilon^+ - E(x) - (\Gamma/\pi)I_2(x, \varepsilon^+))^2} \quad (\text{A.18})$$

A.3 Away from half filling

We proceed by generalizing the variational solution to the case with no p-h symmetry (still assuming no SOC and no direct tunneling). First, we write the Hamiltonian as a sum of the p-h symmetric and antisymmetric terms:

$$H = H_s + H_a. \quad (\text{A.19})$$

We parametrize the deviation from the p-h symmetric point as $\nu = 1 + \delta$ and write (up to a constant):

$$H_a = -U\delta \sum_\sigma \left(n_\sigma - \frac{1}{2} \right). \quad (\text{A.20})$$

Non-zero δ results in additional terms in the variational equations.

$$\begin{aligned} \text{A.1} \quad & += a^\mp U\delta, \\ \text{A.2} \quad & += 0, \\ \text{A.3} \quad & += 0, \\ \text{A.4} \quad & += \beta_{llkk'}^\mp U\delta, \\ \text{A.5} \quad & += \beta_{LRkk'}^\mp U\delta. \end{aligned} \quad (\text{A.21})$$

These terms break the η -symmetry and result in coupling between the ABS-like states from different parity sectors. In practice, this means that variational solutions cannot be expressed

⁴Deep in the YSR regime, at large values of Γ , $|\beta|^2$ become comparable to $|a|^2$

in terms of two separate eigenvalue equations (like in Eqs. (A.12), (A.13)) but rather as solutions to a 2×2 non-linear eigenvalue problem. To avoid solving the non-linear eigenvalue problem, we turn to a conceptually more transparent way of assessing the effect of H_a .

If the parameters are such that both subgap states lie sufficiently deep in the continuum, H_a can be treated within a two-level approximation, its effect reduced to the coupling of the η -even and η -odd states:

$$H = \begin{bmatrix} \epsilon^+ & (a^+)^* a^- U \delta \\ a^+ (a^-)^* U \delta & \epsilon^- \end{bmatrix} \quad (\text{A.22})$$

in the basis of the variational wavefunctions in the p-h symmetric case. The main effect of $\nu \neq 1$ is thus level repulsion. The change in eigenenergies is easily expressed in terms of unperturbed energies ϵ^\pm :

$$\epsilon_{G,E} = \frac{\epsilon^+ + \epsilon^-}{2} \mp \sqrt{\left(\frac{\epsilon^+ - \epsilon^-}{2}\right)^2 + (|a^+||a^-|U\delta)^2} \quad (\text{A.23})$$

Moreover, after finding the eigenvectors, \mathbf{v}_G and \mathbf{v}_E of H , we are able to extract the properties of the wavefunction at $\nu \neq 1$. For example, the probability of the single-electron occupancy on the dot is given by:

$$P_{1,G/E} = 2 \sum_{lk} |\alpha_{lk}|^2 = 1 - (|a^+ v_{G/E,1}|^2 + |a^- v_{G/E,2}|^2), \quad (\text{A.24})$$

where $v_{G/E,i}$ is one of the two vector components.

A.4 Background tunneling processes

If $V^{(D)}$ is non-zero, the following additional terms need to be added to the variational equations:

$$\text{A.1} \quad += \frac{\sqrt{2}V^{(D)}}{N} \sum_{k,k'} \beta_{LRkk'}^\pm (v_{Lk}^* u_{Rk'}^* + u_{Lk}^* v_{Rk'}^*), \quad (\text{A.25})$$

$$\text{A.2} \quad += \frac{V^{(D)}}{N} \sum_{k'} \alpha_{Rk'} (u_{Lk} u_{Rk'}^* - v_{Lk} v_{Rk'}^*), \quad (\text{A.26})$$

$$\text{A.3} \quad += \frac{V^{(D)}}{N} \sum_{k'} \alpha_{Lk'} (u_{Rk} u_{Lk'}^* - v_{Rk} v_{Lk'}^*), \quad (\text{A.27})$$

$$\text{A.4} \quad += \frac{V^{(D)}}{\sqrt{2}N} \sum_q \left[\beta_{LRk'q}^\pm (u_{Lk} u_{Rq}^* - v_{Lk} v_{Rq}^*) + \beta_{LRkq}^\pm (u_{Lk'} u_{Rq}^* - v_{Lk'} v_{Rq}^*) \right], \quad (\text{A.28})$$

$$\text{A.5} \quad += \frac{\sqrt{2}V^{(D)}}{N} \sum_q \left[\beta_{LLqk}^\pm (u_{Rk'} u_{Lq}^* - v_{Rk'} v_{Lq}^*) + \beta_{RRqk'}^\pm (u_{Lk} u_{Rq}^* - v_{Lk} v_{Rq}^*) + a^\pm (v_{Lk} u_{Rk'} + u_{Lk} v_{Rk'}) \right]. \quad (\text{A.29})$$

To assess the phase dependence, we estimate the coherence factors using their values at the bottom of the conduction band. This corresponds to retaining the lowest Fourier modes only.

We find

$$\text{A.1} \quad += \frac{\sqrt{2}V^{(D)}}{N} \sum_{k,k'} \beta_{LRkk'}^\pm \cos(\phi/2), \quad (\text{A.30})$$

$$\text{A.2} \quad += \frac{V^{(D)}}{N} \sum_{k'} \alpha_{Rk'} (\mp i \sin(\phi/2)), \quad (\text{A.31})$$

$$\text{A.3} \quad += \frac{V^{(D)}}{N} \sum_{k'} \alpha_{Lk'} (\mp i \sin(\phi/2)), \quad (\text{A.32})$$

$$\text{A.4} \quad += \frac{V^{(D)}}{\sqrt{2}N} \sum_q (\beta_{LRk'q}^\pm + \beta_{LRkq}^\pm) (\mp i \sin(\phi/2)), \quad (\text{A.33})$$

$$\text{A.5} \quad += \frac{\sqrt{2}V^{(D)}}{N} \sum_q [(\beta_{LLqk}^\pm - \beta_{RRqk'}^\pm) (\mp i \sin(\phi/2)) + a^\pm \cos(\phi/2)]. \quad (\text{A.34})$$

Eq. (A.30) and the last term in Eq. (A.34) show that zero-QP and two-QP states (LR) are coupled via interlead tunneling. This corresponds to Cooper pair breaking and recombination processes, which occur for all $\phi \neq \pi$. Eqs. (A.31) and (A.32) correspond to the mixing between the L and R combinations of YSR states. These processes explicitly break the symmetry of the coefficients $\alpha_{L/R}$ with respect to the Fermi level, thus it is no longer possible to form the linear combinations that allowed us to form the even and odd combinations to make use of the η -symmetry in reducing the problem. They thus embody the breaking of p-h symmetry by the direct tunneling. Such processes are present for all non-zero values of the phase bias ϕ . Finally, there exists three-way mixing for 2-QP states described in Eq. (A.33) and the first part of Eq. (A.34), involving LL, RR, and LR configurations, but the effect of these 2-QP contributions is less significant.

A.5 Spin-orbit coupling

As a last step, we now consider the spin-flip tunneling terms. The equations for the singlet terms are extended as follows:

$$\text{A.1} \quad += -\frac{V_L^{(\text{SF})}}{\sqrt{N}} \sum_k \alpha_{Lk}^T (v_{Lk}^* \pm u_{Lk}^*) + \frac{V_R^{(\text{SF})}}{\sqrt{N}} \sum_k \alpha_{Rk}^T (v_{Rk}^* \pm u_{Rk}^*), \quad (\text{A.35})$$

$$\begin{aligned} \text{A.2} \quad += & -\frac{V_L^{(\text{SF})}}{\sqrt{N}} \sum_{k'} (u_{Lk'}^* - v_{Lk'}^*) \xi_{LLkk'}^+ - \frac{V_L^{(\text{SF})}}{\sqrt{N}} \sum_{k'} (u_{Lk'}^* + v_{Lk'}^*) \xi_{LLkk'}^- \\ & + \frac{V_R^{(\text{SF})}}{\sqrt{N}} \sum_{k'} (u_{Rk'}^* - v_{Rk'}^*) \xi_{LRkk'}^+ + \frac{V_R^{(\text{SF})}}{\sqrt{N}} \sum_{k'} (u_{Rk'}^* + v_{Rk'}^*) \xi_{LRkk'}^-, \end{aligned} \quad (\text{A.36})$$

$$\text{A.3} \quad \text{as above with } L \leftrightarrow R, \quad (\text{A.37})$$

$$\text{A.4} \quad += -\frac{V_l^{(\text{SF})}}{2\sqrt{N}} \alpha_{lk}^T (u_{lk'} \mp v_{lk'}) - \frac{V_l^{(\text{SF})}}{2\sqrt{N}} \alpha_{lk'}^T (u_{lk} \mp v_{lk}), \quad (\text{A.38})$$

$$\text{A.5} \quad += \frac{V_R^{(\text{SF})}}{\sqrt{2}N} \alpha_{Lk}^T (u_{Rk'} \mp v_{Rk'}) - \frac{V_L^{(\text{SF})}}{\sqrt{2}N} \alpha_{Rk'}^T (u_{Lk} \mp v_{Lk}). \quad (\text{A.39})$$

The new equations for the triplet terms are

$$\begin{aligned}
(\epsilon - E_{Lk}) \alpha_{Lk}^T &= \frac{V_L^{(\text{SF})}}{\sqrt{N}} a^+ (v_{Lk} + u_{Lk}) + \frac{V_L^{(\text{SF})}}{\sqrt{N}} a^- (v_{Lk} - u_{Lk}) \\
&\quad - \frac{V_L^{(\text{N})}}{\sqrt{N}} \sum_{k'} (u_{Lk'}^* - v_{Lk'}^*) \xi_{LLkk'}^+ - \frac{V_L^{(\text{N})}}{\sqrt{N}} \sum_{k'} (u_{Lk'}^* + v_{Lk'}^*) \xi_{LLkk'}^- \\
&\quad - \frac{V_R^{(\text{N})}}{\sqrt{2N}} \sum_{k'} (u_{Rk'}^* - v_{Rk'}^*) \xi_{LRkk'}^+ - \frac{V_R^{(\text{N})}}{\sqrt{2N}} \sum_{k'} (u_{Rk'}^* + v_{Rk'}^*) \xi_{LRkk'}^- \\
&\quad + \frac{V_L^{(\text{SF})}}{\sqrt{N}} \sum_{k'} (u_{Lk'}^* - v_{Lk'}^*) \beta_{LLkk'}^+ + \frac{V_L^{(\text{SF})}}{\sqrt{N}} \sum_{k'} (u_{Lk'}^* + v_{Lk'}^*) \beta_{LLkk'}^- \\
&\quad - \frac{V_R^{(\text{SF})}}{\sqrt{2N}} \sum_{k'} (u_{Rk'}^* - v_{Rk'}^*) \beta_{LRkk'}^+ - \frac{V_R^{(\text{SF})}}{\sqrt{2N}} \sum_{k'} (u_{Rk'}^* + v_{Rk'}^*) \beta_{LRkk'}^- \\
&\quad + \frac{V^{(\text{D})}}{N} \sum_{k'} \alpha_{Rk'}^T (u_{Lk} u_{Rk'}^* - v_{Lk} v_{Lk'}^*),
\end{aligned} \tag{A.40}$$

$$\begin{aligned}
\left(\epsilon - \frac{U}{2} - E_{Lk} - E_{Lk'} \right) \xi_{LLkk'}^\pm &= -\frac{V_L^{(\text{N})}}{2\sqrt{N}} \alpha_{Lk}^T (u_{Lk'} \mp v_{Lk'}) + \frac{V_L^{(\text{N})}}{2\sqrt{N}} \alpha_{Lk'}^T (u_{Lk} \mp v_{Lk}) \\
&\quad - \frac{V_L^{(\text{SF})}}{2\sqrt{N}} \alpha_{Lk} (u_{Lk'} \mp v_{Lk'}) - \frac{V_L^{(\text{SF})}}{2\sqrt{N}} \alpha_{Lk'} (u_{Lk} \mp v_{Lk}) \\
&\quad + U \delta \xi_{LLkk'}^\mp \\
&\quad + \frac{V^{(\text{D})}}{\sqrt{2N}} \sum_q \left[u_{Rq}^* (u_{Lk'} \xi_{LRkq} - u_{Lk} \xi_{LRk'q}) \right. \\
&\quad \left. + v_{Rq}^* (-v_{Lk'} \xi_{LRkq} + v_{Lk} \xi_{LRk'q}) \right].
\end{aligned} \tag{A.41}$$

$$\begin{aligned}
\left(\epsilon - \frac{U}{2} - E_{Lk} - E_{Rk'} \right) \xi_{LRkk'}^\pm &= \frac{V_L^{(\text{N})}}{\sqrt{2N}} \alpha_{Rk'}^T (u_{Lk} \mp v_{Lk}) - \frac{V_R^{(\text{N})}}{\sqrt{2N}} \alpha_{Lk}^T (u_{Rk'} \mp v_{Rk'}) \\
&\quad - \frac{V_L^{(\text{SF})}}{\sqrt{2N}} \alpha_{Rk'} (u_{Lk} \mp v_{Lk}) - \frac{V_L^{(\text{SF})}}{\sqrt{2N}} \alpha_{Lk} (u_{Rk'} \mp v_{Rk'}) \\
&\quad + U \delta \xi_{LRkk'}^\mp \\
&\quad - \frac{\sqrt{2} V^{(\text{D})}}{N} \sum_q \left[(v_{Lq}^* v_{Rk'} - u_{Lq}^* u_{Rk'}) \xi_{LLkq} - (v_{Rq}^* v_{Lk} - u_{Rq}^* u_{Lk}) \xi_{RRk'q} \right].
\end{aligned} \tag{A.42}$$

To solve this fully general variational problem, one can proceed by analogy with the simpler cases considered previously. The set of equations can be reduced to four equations for $\alpha_{L,R}$ and $\alpha_{L,R}^T$ by substituting coefficients a^\pm , as well as β and ξ functions. One then derives a characteristic equation for this 4×4 eigenvalue problem. The resulting transcendental equation can be solved numerically.

References

- [1] N. M. Chtchelkatchev and Y. V. Nazarov, *Andreev quantum dots for spin manipulation*, Physical Review Letters **90**(22) (2003).

- [2] C. Padurariu and Y. V. Nazarov, *Theoretical proposal for superconducting spin qubits*, Physical Review B **81**(14), 144519 (2010).
- [3] M. Hays, V. Fatemi, D. Bouman, J. Cerrillo, S. Diamond, K. Serniak, T. Connolly, P. Krogstrup, J. Nygård, A. L. Yeyati, A. Geresdi and M. H. Devoret, *Coherent manipulation of an Andreev spin qubit*, Science **373**(6553), 430 (2021).
- [4] A. Bargerbos, M. Pita-Vidal, R. Žitko, J. Ávila, L. J. Splitthoff, L. Grünhaupt, J. J. Wesdorp, C. K. Andersen, Y. Liu, L. P. Kouwenhoven, R. Aguado, A. Kou *et al.*, *Singlet-doublet transitions of a quantum dot Josephson junction detected in a transmon circuit*, PRX Quantum **3**(3) (2022), doi:[10.1103/prxquantum.3.030311](https://doi.org/10.1103/prxquantum.3.030311).
- [5] A. Bargerbos, M. Pita-Vidal, R. Žitko, L. J. Splitthoff, L. Grünhaupt, J. J. Wesdorp, Y. Liu, L. P. Kouwenhoven, R. Aguado, C. K. Andersen, A. Kou and B. van Heck, *Spectroscopy of spin-split Andreev levels in a quantum dot with superconducting leads*, Physical Review Letters **131**(9), 097001 (2023), doi:[10.1103/physrevlett.131.097001](https://doi.org/10.1103/physrevlett.131.097001).
- [6] M. Pita-Vidal, A. Bargerbos, R. Žitko, L. J. Splitthoff, L. Grünhaupt, J. J. Wesdorp, Y. Liu, L. P. Kouwenhoven, R. Aguado, B. van Heck, A. Kou and C. K. Andersen, *Direct manipulation of a superconducting spin qubit strongly coupled to a transmon qubit*, Nature Physics (2023), doi:[10.1038/s41567-023-02071-x](https://doi.org/10.1038/s41567-023-02071-x).
- [7] M. Pita-Vidal, J. J. Wesdorp and C. K. Andersen, *Blueprint for all-to-all-connected superconducting spin qubits*, PRX Quantum **6**(1), 010308 (2025), doi:[10.1103/prxquantum.6.010308](https://doi.org/10.1103/prxquantum.6.010308).
- [8] A. Zazunov, V. S. Shumeiko, E. N. Bratus', J. Lantz and G. Wendin, *Andreev level qubit*, Physical Review Letters **90**(8) (2003).
- [9] L. Bretheau, u. O. Girit, H. Pothier, D. Esteve and C. Urbina, *Exciting Andreev pairs in a superconducting atomic contact*, Nature **499**(7458), 312–315 (2013), doi:[10.1038/nature12315](https://doi.org/10.1038/nature12315).
- [10] L. Bretheau, C. O. Girit, C. Urbina, D. Esteve and H. Pothier, *Supercurrent spectroscopy of Andreev states*, Phys. Rev. X **3**, 041034 (2013).
- [11] C. Janvier, L. Tosi, L. Bretheau, C. O. Girit, M. Stern, P. Bertet, P. Joyez, D. Vion, D. Esteve, M. F. Goffman, H. Pothier and C. Urbina, *Coherent manipulation of Andreev states in superconducting atomic contacts*, Science **349**, 1199 (2015).
- [12] M. Hays, G. de Lange, K. Serniak, D. J. van Woerkom, D. Bouman, P. Krogstrup, J. Nygård, A. Geresdi and M. H. Devoret, *Direct microwave measurement of Andreev-bound-state dynamics in a semiconductor-nanowire Josephson junction*, Physical Review Letters **121**(4) (2018).
- [13] L. Tosi, C. Metzger, M. F. Goffman, C. Urbina, H. Pothier, S. Park, A. L. Yeyati, J. Nygård and P. Krogstrup, *Spin-orbit splitting of Andreev states revealed by microwave spectroscopy*, Physical Review X **9**(1), 011010 (2019).
- [14] C. Metzger, S. Park, L. Tosi, C. Janvier, A. A. Reynoso, M. F. Goffman, C. Urbina, A. L. Yeyati and H. Pothier, *Circuit-QED with phase-biased Josephson weak links*, Physical Review Research **3**(1), 013036 (2021).

- [15] L. Y. Cheung, R. Haller, A. Kononov, C. Ciaccia, J. H. Ungerer, T. Kanne, J. Nygård, P. Winkel, T. Reisinger, I. M. Pop, A. Baumgartner and C. Schönenberger, *Photon-mediated long-range coupling of two Andreev pair qubits*, *Nature Physics* **20**(11), 1793–1797 (2024), doi:[10.1038/s41567-024-02630-w](https://doi.org/10.1038/s41567-024-02630-w).
- [16] O. Shvetsov, A. Khola, V. Buccheri, I. Cools, N. Trnjanin, A. Geresd, T. Kanne and J. Nard, *Approaching the ultrastrong coupling regime between an Andreev level and a microwave resonator*, 2502.09243 (2025).
- [17] G. de Lange, B. van Heck, A. Bruno, D. J. van Woerkom, A. Geresdi, S. R. Plissard, E. P. A. M. Bakkers, A. R. Akhmerov and L. DiCarlo, *Realization of microwave quantum circuits using hybrid superconducting-semiconducting nanowire Josephson elements*, *Physical Review Letters* **115**(12) (2015).
- [18] T. W. Larsen, K. D. Petersson, F. Kuemmeth, T. S. Jespersen, P. Krogstrup, J. Nygård and C. M. Marcus, *Semiconductor-nanowire-based superconducting qubit*, *Physical Review Letters* **115**(12) (2015).
- [19] P. Zellekens, R. S. Deacon, P. Perla, D. Grützmacher, M. I. Lepsa, T. Schäpers and K. Ishibashi, *Microwave spectroscopy of Andreev states in InAs nanowire-based hybrid junctions using a flip-chip layout*, *Communications Physics* **5**(1), 267 (2022), doi:[10.1038/s42005-022-01035-6](https://doi.org/10.1038/s42005-022-01035-6).
- [20] S. C. ten Kate, D. C. Ohnmacht, M. Coraiola, T. Antonelli, S. Paredes, F. J. Schupp, M. Hinderling, S. W. Bedell, W. Belzig, J. C. Cuevas, A. E. Svetogorov, F. Nichele *et al.*, *Finite length effects and coulomb interaction in Ge quantum well-based Josephson junctions probed with microwave spectroscopy*, *Physical Review Applied* **24**(6), 064005 (2025), doi:[10.1103/hb1h-8jn9](https://doi.org/10.1103/hb1h-8jn9).
- [21] S. D. Franceschi, L. Kouwenhoven, C. Schönenberger and W. Wernsdorfer, *Hybrid superconductor-quantum dot devices*, *Nat. Nanotechnology* **5**, 703 (2010).
- [22] V. Meden, *The Anderson-Josephson quantum dot – a theory perspective*, *J. Phys.: Condens. Matter* **31**, 163001 (2019).
- [23] J.-D. Pillet, P. Joyez, R. Žitko and M. F. Goffman, *Tunneling spectroscopy of a single quantum dot coupled to a superconductor: From Kondo ridge to Andreev bound states*, *Phys. Rev. B* **88**, 045101 (2013).
- [24] E. J. H. Lee, X. Jiang, R. Žitko, R. Aguado, C. M. Lieber and S. De Franceschi, *Scaling of subgap excitations in a superconductor-semiconductor nanowire quantum dot*, *Phys. Rev. B* **95**, 180502(R) (2017).
- [25] G. Kiršanskas, M. Goldstein, K. Flensberg, L. I. Glazman and J. Paaske, *Yu-Shiba-Rusinov states in phase-biased superconductor-quantum dot-superconductor junctions*, *Physical Review B* **92**(23), 235422 (2015), doi:[10.1103/physrevb.92.235422](https://doi.org/10.1103/physrevb.92.235422).
- [26] A. Jellinggaard, K. Grove-Rasmussen, M. H. Madsen and J. Nygård, *Tuning Yu-Shiba-Rusinov states in a quantum dot*, *Phys. Rev. B* **94**, 064520 (2016).
- [27] T. Ilićin and R. Žitko, *Variational solution of the superconducting Anderson impurity model and the band-edge singularity phenomena*, *SciPost Physics* **19**(1) (2025), doi:[10.21468/scipostphys.19.1.006](https://doi.org/10.21468/scipostphys.19.1.006).

- [28] P. D. Kurilovich, V. D. Kurilovich, V. Fatemi, M. H. Devoret and L. I. Glazman, *Microwave response of an Andreev bound state*, Physical Review B **104**(17), 174517 (2021), doi:[10.1103/PhysRevB.104.174517](https://doi.org/10.1103/PhysRevB.104.174517).
- [29] V. Fatemi, P. D. Kurilovich, M. Hays, D. Bouman, T. Connolly, S. Diamond, N. E. Frattini, V. D. Kurilovich, P. Krogstrup, J. Nygård, A. Geresdi, L. I. Glazman *et al.*, *Microwave susceptibility observation of interacting many-body Andreev states*, Physical Review Letters **129**(22), 227701 (2022), doi:[10.1103/PhysRevLett.129.227701](https://doi.org/10.1103/PhysRevLett.129.227701).
- [30] F. J. Matute-Cañadas, C. Metzger, S. Park, L. Tosi, P. Krogstrup, J. Nygård, M. F. Goffman, C. Urbina, H. Pothier and A. Levy Yeyati, *Signatures of interactions in the Andreev spectrum of nanowire Josephson junctions*, Physical Review Letters **128**(19), 197702 (2022), doi:[10.1103/PhysRevLett.128.197702](https://doi.org/10.1103/PhysRevLett.128.197702).
- [31] L. Pavešić, M. Pita Vidal, A. Bargerbos and R. Žitko, *Impurity Knight shift in quantum dot Josephson junctions*, SciPost Phys. **15**, 070 (2023), doi:[10.21468/SciPostPhys.15.2.070](https://doi.org/10.21468/SciPostPhys.15.2.070).
- [32] P. D. Kurilovich, V. D. Kurilovich, A. E. Svetogorov, W. Belzig, M. H. Devoret and L. I. Glazman, *On-demand population of Andreev levels by their ionization in the presence of Coulomb blockade*, Physical Review B **110**(18), 184508 (2024), doi:[10.1103/PhysRevB.110.184508](https://doi.org/10.1103/PhysRevB.110.184508).
- [33] J. J. Wesdorp, F. J. Matute-Cañadas, A. Vaartjes, L. Grünhaupt, T. Laeven, S. Roelofs, L. J. Splitthoff, M. Pita-Vidal, A. Bargerbos, D. J. van Woerkom, P. Krogstrup, L. P. Kouwenhoven *et al.*, *Microwave spectroscopy of interacting Andreev spins*, Physical Review B **109**(4), 045302 (2024), doi:[10.1103/physrevb.109.045302](https://doi.org/10.1103/physrevb.109.045302).
- [34] A. Bordin, F. J. B. Evertsz, G. O. Steffensen, T. Dvir, G. P. Mazur, D. van Driel, N. van Loo, J. C. Wolff, E. P. A. M. Bakkers, A. L. Yeyati and L. P. Kouwenhoven, *Impact of Andreev bound states within the leads of a quantum dot Josephson junction*, Physical Review X **15**(1), 011046 (2025), doi:[10.1103/PhysRevX.15.011046](https://doi.org/10.1103/PhysRevX.15.011046).
- [35] A. Zazunov, R. Egger, T. Jonckheere and T. Martin, *Anomalous Josephson current through a spin-orbit coupled quantum dot*, Physical Review Letters **103**(14), 147004 (2009), doi:[10.1103/physrevlett.103.147004](https://doi.org/10.1103/physrevlett.103.147004).
- [36] A. A. Reynoso, G. Usaj, C. A. Balseiro, D. Feinberg and M. Avignon, *Spin-orbit-induced chirality of Andreev states in Josephson junctions*, Physical Review B **86**(21), 214519 (2012), doi:[10.1103/physrevb.86.214519](https://doi.org/10.1103/physrevb.86.214519).
- [37] B. Béri, J. H. Bardarson and C. W. J. Beenakker, *Splitting of Andreev levels in a Josephson junction by spin-orbit coupling*, Physical Review B **77**(4) (2008).
- [38] B. van Heck, J. I. Väyrynen and L. I. Glazman, *Zeeman and spin-orbit effects in the Andreev spectra of nanowire junctions*, Physical Review B **96**(7), 075404 (2017), doi:[10.1103/physrevb.96.075404](https://doi.org/10.1103/physrevb.96.075404).
- [39] M. Hays, V. Fatemi, K. Serniak, D. Bouman, S. Diamond, G. de Lange, P. Krogstrup, J. Nygård, A. Geresdi and M. H. Devoret, *Continuous monitoring of a trapped superconducting spin*, Nature Physics **16**(11), 1103 (2020), doi:[10.1038/s41567-020-0952-3](https://doi.org/10.1038/s41567-020-0952-3).
- [40] K. Zatsaryna, A. Nava, A. Zazunov and R. Egger, *Many-body quantum dynamics of spin-orbit coupled Andreev states in a zeeman field*, Physical Review B **109**(21), 214505 (2024), doi:[10.1103/physrevb.109.214505](https://doi.org/10.1103/physrevb.109.214505).

- [41] M. Amundsen, J. Linder, J. W. Robinson, I. Žutić and N. Banerjee, *Colloquium : Spin-orbit effects in superconducting hybrid structures*, *Reviews of Modern Physics* **96**(2) (2024), doi:[10.1103/revmodphys.96.021003](https://doi.org/10.1103/revmodphys.96.021003).
- [42] V. Fatemi, P. Kurilovich, M. Hays, D. Bouman, T. Connolly, S. Diamond, N. Frattini, V. Kurilovich, P. Krogstrup, J. Nygård, A. Geresdi, L. Glazman *et al.*, *Microwave susceptibility observation of interacting many-body Andreev states*, *Physical Review Letters* **129**(22), 227701 (2022), doi:[10.1103/physrevlett.129.227701](https://doi.org/10.1103/physrevlett.129.227701).
- [43] F. Matute-Cañadas, C. Metzger, S. Park, L. Tosi, P. Krogstrup, J. Nygård, M. Goffman, C. Urbina, H. Pothier and A. L. Yeyati, *Signatures of interactions in the Andreev spectrum of nanowire Josephson junctions*, *Physical Review Letters* **128**(19), 197702 (2022), doi:[10.1103/physrevlett.128.197702](https://doi.org/10.1103/physrevlett.128.197702).
- [44] E. Vecino, A. Martín-Rodero and A. Yeyati, *Josephson current through a correlated quantum level: Andreev states and pi junction behavior*, *Phys. Rev. B* **68**, 035105 (2003).
- [45] V. V. Baran, E. J. P. Frost and J. Paaske, *Surrogate model solver for impurity-induced superconducting subgap states*, *Physical Review B* **108**(22), L220506 (2023), doi:[10.1103/physrevb.108.l220506](https://doi.org/10.1103/physrevb.108.l220506).
- [46] K. G. Wilson, *The renormalization group: Critical phenomena and the Kondo problem*, *Rev. Mod. Phys.* **47**, 773 (1975).
- [47] R. Bulla, T. A. Costi and T. Pruschke, *The numerical renormalization group method for quantum impurity systems*, *Rev. Mod. Phys.* **80**, 395 (2008).
- [48] R. Žitko and T. Pruschke, *Energy resolution and discretization artefacts in the numerical renormalization group*, *Phys. Rev. B* **79**, 085106 (2009).
- [49] R. Žitko, M. Lee, R. Lopez, R. Aguado and M.-S. Choi, *Josephson current in strongly correlated double quantum dots*, *Phys. Rev. Lett.* **105**, 116803 (2010).
- [50] P. Zalom, D. Rolih and R. Žitko, *Andreev bound state spectroscopy of a quantum-dot-based Aharonov-Bohm interferometer with superconducting terminals*, arxiv:2507.03614 (2025).
- [51] L. Pavešić, R. Aguado and R. Žitko, *Strong-coupling theory of quantum-dot Josephson junctions: Role of a residual quasiparticle*, *Physical Review B* **109**(12), 125131 (2024), doi:[10.1103/physrevb.109.125131](https://doi.org/10.1103/physrevb.109.125131).
- [52] Q.-H. W. Jin-Guo Liu, Da Wang, *Quantum impurities in channel mixing baths*, *Phys. Rev. B* **93**, 035102 (2016).
- [53] P. Zalom, *Rigorous Wilsonian renormalization group for impurity models with a spectral gap*, *Physical Review B* **108**(19) (2023), doi:[10.1103/physrevb.108.195123](https://doi.org/10.1103/physrevb.108.195123).
- [54] R. Žitko and L. Pavešić, *Yu-Shiba-Rusinov states, BCS-BEC crossover, and exact solution in the flat-band limit*, *Physical Review B* **106**(2), 024513 (2022).
- [55] S. Park and A. L. Yeyati, *Andreev spin qubits in multichannel Rashba nanowires*, *Physical Review B* **96**(12), 125416 (2017).
- [56] S. Park, C. Metzger, L. Tosi, M. F. Goffman, C. Urbina, H. Pothier and A. L. Yeyati, *From adiabatic to dispersive readout of quantum circuits*, *Physical Review Letters* **125**(7), 077701 (2020), doi:[10.1103/physrevlett.125.077701](https://doi.org/10.1103/physrevlett.125.077701).

- [57] Y. Fauvel, J. S. Meyer and M. Houzet, *Opportunities for the direct manipulation of a phase-driven Andreev spin qubit*, *Physical Review B* **109**(18), 184515 (2024), doi:[10.1103/physrevb.109.184515](https://doi.org/10.1103/physrevb.109.184515).
- [58] J. C. E. Saldaña, A. Vekris, L. Pavešić, P. Krogstrup, R. Žitko, K. Grove-Rasmussen and J. Nygård, *Excitations in a superconducting Coulombic energy gap*, *Nat. Commun.* **13**, 2243 (2022).